bioRxiv preprint doi: https://doi.org/10.1101/2023.01.23.525164; this version posted January 23, 2023. The copyright holder for this preprint (which was not certified by peer review) is the author/funder, who has granted bioRxiv a license to display the preprint in perpetuity. It is made available under aCC-BY-NC-ND 4.0 International license.

N-glycosylation engineering in chimeric antigen receptor T cells enhances anti-tumor activity

Elien De Bousser[1,2,4*°] & Nele Festjens[1,2,4*], Leander Meuris[1,2,4], Evelyn Plets[1,2], Annelies Van Hecke[1,2], Elise Wyseure[1,2], Stijn De Munter[3,4], Bart Vandekerckhove[3,4], Nico Callewaert[1,2,4°]

[*]These authors contributed equally to this work

°Correspondence should be addressed to NC (Nico.Callewaert@vib-ugent.be) and EDB (Elien.DeBousser@vib-ugent.be)

[1]VIB-UGent Center for Medical Biotechnology

[2]Department for Biochemistry and Microbiology, Ghent University

Technologiepark-Zwijnaarde 75, B-9052 Gent, Belgium

[3]Department of Diagnostic Sciences, Ghent University, 9000 Ghent, Belgium

[4]Cancer Research Institute Ghent (CRIG), Ghent, Belgium

Author contributions

EDB and NF were responsible for the experimental design and data analysis. EDB, NF, EP, AVH and EW acquired the data. LM performed the statistical analyses. SDM designed the CD70 nanoCAR and set up the assays for functional analysis under the supervision of BV. NC initiated and supervised the project and manuscript writing.

bioRxiv preprint doi: https://doi.org/10.1101/2023.01.23.525164; this version posted January 23, 2023. The copyright holder for this preprint (which was not certified by peer review) is the author/funder, who has granted bioRxiv a license to display the preprint in perpetuity. It is made available under aCC-BY-NC-ND 4.0 International license.

Abstract

Recently, chimeric antigen receptor (CAR) T cell technology has revolutionized cancer immunotherapy. This strategy uses synthetic CARs to redirect T cells to specific antigens expressed on the surface of tumor cells. Despite impressive progress in the treatment of hematological malignancies with CAR T cells, scientific challenges still remain for use of CAR T cell therapy to treat solid tumors. This is mainly due to the hostile tumor microenvironment and CAR-related toxicities. As the glycans decorating the T cell surface are implicated in T cell activation, differentiation, proliferation, and in the interaction of human T cells with tumor cells, we studied the role of human T cell glycosylation in more depth by manipulating their glycome. In this context, there is *in vitro* evidence that β-galactoside binding lectins (Galectins) can have a strong impact on the functionality of tumor-infiltrating T cells. The high-affinity poly-LacNAc N-linked galectin ligands are mainly synthesized onto the β1,6-GlcNAc branch introduced by N-acetylglucosaminyltransferase V (GnTV, encoded by *Mgat5*). We showed that knocking out *Mgat5* in CD70 targeting CAR T cells leads to lower densities of poly-LacNAc modifications on the CAR T cell surface. Most interestingly, our results indicate that MGAT5 KO CD70 CAR T cells show enhanced potency to control primary tumors and relapses.

bioRxiv preprint doi: https://doi.org/10.1101/2023.01.23.525164; this version posted January 23, 2023. The copyright holder for this preprint (which was not certified by peer review) is the author/funder, who has granted bioRxiv a license to display the preprint in perpetuity. It is made available under aCC-BY-NC-ND 4.0 International license.

Introduction

Immunotherapy with T cells that are genetically modified to express chimeric antigen receptors (CARs), which target tumor-associated molecules, has shown impressive efficacy in several malignancies[1]. The advent of second-generation CAR T cells, in which activating and costimulatory signaling domains are combined, has led to encouraging results in patients with chemo-refractory B cell malignancies[2,3]. However, the translation of this clinical success to the treatment of solid tumors requires overcoming multiple obstacles[4]. In general, it is required to generate robust and stable populations of T cells that are able to infiltrate the tumor and escape the immunosuppressive effect of the tumor microenvironment (TME). Further issues in CAR T cell therapy include antigen escape, CAR T cell therapy-related toxicities and the relatively high occurrence of tumor relapse.

Cell surface glycosylation plays an important role in the interaction of human T cells with tumor cells and often contributes to escape mechanisms adopted by the tumor to evade T cell anti-tumor immunity[5]. For example, the expression of immune checkpoint inhibitors such as PD-1 and CTLA-4 is tuned by glycosylation[6–8]. Further, there is *in vitro* evidence that β-galactoside binding lectins (Galectins) can have a strong impact on the functionality of tumor-infiltrating T cells[9]. Galectin-1 controls T cell effector function homeostasis by regulating activation, differentiation, survival and cytokine production[10]. Galectin-9 is one of the ligands of Tim-3 and negatively regulates T cell immunity[11]. Binding of Galectin-3 to glycoproteins has both pro- and anti-apoptotic effects on T cells, depending on its localization. Intracellular Galectin-3 blocks apoptosis by stabilizing the mitochondrial membrane and preventing cytochrome c release,[12] while extracellular Galectin-3 binds to glycoproteins such as CTLA-4 and Lag3 on the T cell surface, leading to inhibition and cell death of activated T cells[13,14]. Endogenous Galectin-3, produced by activated T cells, is recruited to the immunological synapse. There it negatively regulates T cell activation by destabilizing the immunological synapse through direct interactions with glycoproteins associated with the T cell receptor, and by promoting downregulation of the TCR[15,16]. Another interesting finding is that binding of Galectin-3 to antigen-specific activated $CD8^+$ T cells inhibits their effector function within the tumor microenvironment[13]. It was shown that Galectin-3 prevents the formation of a functional secretory synapse by trapping LFA-1 in glycan-Galectin lattices, leading to reduced cytokine secretion[17]. *Ex vivo* treatment of T cells with an anti-Galectin-3 antibody or a Galectin competitive binder such as N-acetyllactosamine (LacNAc) resulted in the detachment of surface Galectin-3 leading to increased cytotoxicity and ability to secrete cytokines such as IFN-γ[9,18].

The high-affinity poly-LacNAc N-linked galectin ligands are mainly synthesized onto the β1,6-GlcNAc branch introduced by N-acetylglucosaminyltransferase V (MGAT5) (**Figure 1**.A). Knocking out *Mgat5* should thus also strongly reduce the density of poly-LacNAc modifications on the cell surface.

bioRxiv preprint doi: https://doi.org/10.1101/2023.01.23.525164; this version posted January 23, 2023. The copyright holder for this preprint (which was not certified by peer review) is the author/funder, who has granted bioRxiv a license to display the preprint in perpetuity. It is made available under aCC-BY-NC-ND 4.0 International license.

MGAT5 deficiency was shown to markedly increase TCR clustering and signaling at the immune synapse, resulting in a lower T cell activation threshold and increased incidence of autoimmune disease *in vivo* and in human[19].

To evaluate the impact of altered cell surface glycosylation on cytotoxic T cell functionality, specifically in a cancer immunotherapy setting, we used CD70 as the CAR target. Nanobodies targeting CD70 have been thoroughly evaluated as antigen-binding module in a CAR format (CD70 nanoCAR) in the lab of Prof. Dr. Bart Vandekerckhove (Department of Clinical Chemistry, Microbiology and Immunology, Ghent University)[20]. We specifically aimed to evaluate the impact of glyco-engineering via *Mgat5* KO on the CAR T cell glycome and on their *in vitro* and *in vivo* activation, proliferation, differentiation and anti-tumor functionality.

We could demonstrate that MGAT5 KO CD70 nanoCAR T cells are functional and even perform better than CD70 nanoCAR T cells, both *in vitro* and *in vivo*. Both the average tumor volume and the tumor growth rate of primary and secondary tumors are significantly lower in the MGAT5 KO CD70 nanoCAR T cell treated group, as compared to the CD70 nanoCAR T cell treated mice. These results show that disrupting N-glycosylation modifications on CAR T cells enhances their capability to control primary tumors and subsequent relapses. Interestingly, MGAT5 KO CD70 nanoCAR T cells are present in higher numbers than CD70 nanoCAR T cells both *in vitro* and in peripheral blood and spleen upon specific antigen recognition.

Results

Engineering of MGAT5 KO CD70 nanoCAR T cells

We optimized a workflow for the combined CRISPR-Cas9 mediated glyco-gene editing and retroviral CAR delivery to purified, activated human $CD3^+$ T cells. The presence of both $CD4^+$ and $CD8^+$ T cell subsets in the final CAR T cell product is indispensable for efficient anti-tumor immunity.

To efficiently combine CRISPR-Cas9-based glyco-gene editing and retroviral CAR delivery, various experimental steps were optimized. Optimal editing and transduction efficiencies were obtained when $CD3^+$ T cells were stimulated with Immunocult for three days, after which activated T cells were first subjected to Cas9 RNP nucleofection, followed by a 1-hit retroviral transduction on the same day. Engineering efficiencies were assessed on day 10. The experimental timeline is depicted in **Figure 1**.B.

CRISPR editing efficiencies were determined by Sanger sequencing of the region of interest followed by ICE analysis, and the mean editing efficiency as percentage insertions and deletions (% indel) for the *Mgat5* locus over multiple experiments was consistently high (exceeding 80% indel) as is depicted in **Figure 1**.C. Flow cytometry was used to measure both CD70 nanoCAR expression and GFP expression as read outs of the retroviral transduction efficiency. High CD70 nanoCAR transduction efficiencies were consistently

bioRxiv preprint doi: https://doi.org/10.1101/2023.01.23.525164; this version posted January 23, 2023. The copyright holder for this preprint (which was not certified by peer review) is the author/funder, who has granted bioRxiv a license to display the preprint in perpetuity. It is made available under aCC-BY-NC-ND 4.0 International license.

obtained over multiple experiments, irrespective of the simultaneous glyco-gene engineering as shown in Figure 1.D.

MGAT5 KO CD70 nanoCAR T cells show an altered glycocalyx

In order to be able to assess the extent of the intended glycosylation changes upon glyco-gene engineering, we developed a lectin-based flow cytometry assay. For the detection of poly-LacNAc structures, we used the lectin from *Datura stramonium* (DSL) (Figure 1.E). This lectin is reported to bind well to LacNAc and oligomers containing repeating LacNAc sequences next to its preferred N-acetylglucosamine oligomer ligand.

When comparing the DSL lectin stain intensity of mock engineered CD70 nanoCAR T cells with that of MGAT5 KO CD70 nanoCAR T cells, we observe a clear reduction in signal, indicating that we successfully eliminated N-glycan β1,6-branching and subsequent elongation of this branch with poly-LacNAc modifications.

As a complementary method to profile the CAR T cell surface glycosylation, we adapted the DSA-FACE method developed in our research group to enable the analysis of cell surface N-glycosylation. We aimed to directly release the N-glycans from the cell surface by applying the PNGaseF digest on living cells in suspension. We established an optimized protocol in which we incubate 1 x 10^6 cells per sample in the presence of 0.125 IU PNGaseF in PBS for 2 hours at 37°C. Subsequently, the cells are removed by centrifugation and the crude digest is labeled with APTS for 1 hour at 70°C. After two rounds of clean-up over Sephadex resin to remove excess label and salts, labeled N-glycans are resuspended in water and analyzed by DSA-FACE. The complete protocol is schematically depicted in Figure 1.F.

When CAR T cells are engineered for MGAT5, the N-glycan profile is clearly different from that of mock-engineered CAR T cells (Figure 1.F). The peaks in P6 disappear while the peaks in P4 show a higher intensity relative to P2 and P3. This shift in electrophoretic mobility is consistent with the removal of one LacNAc unit (two monosaccharide units) or a shift from a tetra-antennary to a tri-antennary N-glycan. These DSA-FACE results are also in agreement with the lectin-staining experiments, where we observed a reduction in DSL staining intensity upon MGAT5 engineering (Figure 1.E). When comparing to the annotated N-glycan profile of human plasma (data not shown), this observation indeed confirms that P6 corresponds to a tetra-antennary N-glycan, while peaks in P4 and P5 correspond to tri-antennary N-glycan structures.

Characterization of the CD70 expressing tumor cell lines

In order to study the anti-tumor functionality of the MGAT5 KO CD70 nanoCAR T cells, two tumor cell lines were used in our studies. THP-1 cells are a M4 subtype acute myeloid leukemia (AML) cell line and SKOV-3 cells are a serous adenocarcinoma cell line. We confirmed the cell surface CD70 expression on these cells

bioRxiv preprint doi: https://doi.org/10.1101/2023.01.23.525164; this version posted January 23, 2023. The copyright holder for this preprint (which was not certified by peer review) is the author/funder, who has granted bioRxiv a license to display the preprint in perpetuity. It is made available under aCC-BY-NC-ND 4.0 International license.

by flow cytometry (**Supplementary Figure 1**.A). Jurkat cells (immortalized line of human T cells) were included as a negative control. Further, we performed the anti-CD70 cell surface staining on non-transduced (NTC) and CD70 nanoCAR transduced $CD3^+$ T cells and did not identify auto-antigen expression.

Galectins exert a broad range of effects during different aspects of T cell-mediated immunity by the formation of lattices on the T cell surface[5]. In anti-tumor immunity, it has been shown that Galectin-1 and Galectin-3 in the TME lead to tolerogenic signaling and immune suppression. LacNAc is the ligand recognized by Galectins and the affinity of the interaction is proportional to the LacNAc content of the glycan structure. We hypothesized that by eliminating MGAT5 expression in order to reduce the poly-LacNAc content on cytotoxic T cells, the inhibitory effect of Galectins on T cell immunity can be reduced. To this end, we first verified that the tumor cell lines used in our study indeed express Galectin-1 and Galectin-3.

Secretion and subsequent cell surface binding of Galectin-1 and -3 was detected by performing a flow cytometry experiment with anti-Galectin-1 and -3 antibodies. The results are shown in **Supplementary Figure 1**.B. As positive control, cells were incubated with recombinant Galectin-1 or -3 before performing the cell surface staining. As a negative control, cell surface Galectin binding was abolished by the addition of the competitive inhibitor lactose. Jurkat cells were included as negative control cells. Galectin-1 expression is detected for both the THP-1 and SKOV-3 cell lines. Further, galectin-3 expression is clearly observed for the SKOV-3 cell line but only slightly for the THP-1 cell line. No secretion and cell surface binding of galectins is seen on primary $CD3^+$ T cells and Jurkat cells. Binding of recombinant Galectin-3 to T cells leads to an increase in signal, while recombinant Galectin-1 does not seem to bind to the primary T cells.

Additionally, we confirmed the expression of Galectin-1 and -3 in tumor sections from tumor-bearing NSG mice (**Supplementary Figure 1**.C). The latter were obtained by ectopically inoculating human SKOV-3 cells. The SKOV-3 tumor model is used in the experiments described below.

MGAT5 KO CD70 nanoCAR T cells are functional *in vitro*

In a first set of experiments, we evaluated the viability and functionality of MGAT5 KO CD70 nanoCAR T cells *in vitro.* Viability is maintained for each condition as is depicted in **Figure 2**.A. After engineering and culturing, most of the cells in the total $CD3^+$ T cell pool are $CD4^+$ T cells. Even with the 4-1BB signal in the CAR construct, which is believed to support a moderate rise in the $CD8^+$ T cell fraction, the CAR T cell groups show a decrease in the $CD8^+$ population. Furthermore, this decrease is even more pronounced when CD70 nanoCAR T cells were CRISPR-Cas9 engineered (both mock Cas9 and MGAT5 KO), which suggests that the viral transduction and nucleofection procedures might affect the growth of $CD8^+$ T cells more than that of $CD4^+$ T cells (**Figure 2**.B)

bioRxiv preprint doi: https://doi.org/10.1101/2023.01.23.525164; this version posted January 23, 2023. The copyright holder for this preprint (which was not certified by peer review) is the author/funder, who has granted bioRxiv a license to display the preprint in perpetuity. It is made available under aCC-BY-NC-ND 4.0 International license.

The antitumor effects of CAR T cells depend on their capacity to secrete cytokines upon exposure to antigens. Therefore, we evaluated the cytokine production of the glyco-engineered CD70 nanoCAR T cells after challenging them with the THP-1 and SKOV-3 target cell lines (**Figure 2**.C-E). Target cells were co-incubated for 16 hours with MGAT5 KO CD70 nanoCAR T cells. Unstimulated cells were included as negative control and Immunocult stimulation was included as positive control. Subsequently, T cells were labelled for intracellular TNF-α, IFN-γ and IL-2. The MGAT5 KO CD70 nanoCAR T cells are able to produce cytokines upon antigen stimulation and the proportion of cytokine-producing cells is similar to, or even higher than what is observed for mock nucleofected CD70 nanoCAR T cells. This cytokine expression is dependent on CD70 nanoCAR expression, given that non-transduced T cells (NTC) fail to express cytokines or express only very low levels in the presence of CD70 positive cells (but do show expression of cytokines after polyclonal Immunocult stimulation).

In order to evaluate the combined proliferative and cytotoxic potential of MGAT5 KO CD70 nanoCAR T cells, T cells were co-cultured with THP-1 target cells at different ratios for a period of 14 days. The number of THP-1 cells left in culture was determined by flow cytometry every three to four days. At day 7, a second challenge was performed by adding target THP-1 cells to the co-cultures. Results obtained with three independent T cell donors are depicted in **Figure 2**.F-I.

Figure 2.F and G shows the results corresponding to an effector/target (E/T) ratio of 0.15, that is 20 000 THP-1 target cells co-cultured with 3000 CD70 nanoCAR effector cells. At this ratio, all target cells get killed by day 4, in the wild-type, mock engineered and MGAT5 KO CD70 nanoCAR T cell conditions (**Figure 2**.F). Even at a very low E/T ratio of 0.015 (20 000 target cells co-cultured with only 300 CD70 nanoCAR T cells), all target cells are eliminated by day 4, irrespective of the engineering condition (**Figure 2**.H).

Most interestingly, from day 11 onwards, at both E/T ratios the number of CD70 nanoCAR T cells is higher for those that are knockout in *Mgat5*, indicating a higher expansion of these glyco-engineered CAR T cells over time **Figure 2**.G and I. We found that, on day 11, the number of MGAT5 KO nanoCAR T cells is about 1.74 times higher (95% CI: 1.36 to 2.21) than the number of nanoCAR T cells starting from the same conditions. On day 14, the number of MGAT5 KO nanoCAR T similarly is about 1.70 times higher (95% CI: 1.33 to 2.18). All these estimates are averaged over the two E/T ratios and the three independent donors.

Treatment of tumor-bearing mice with MGAT5 KO CAR T cells leads to a better outcome in terms of tumor control

After validating the *in vitro* activity of MGAT5 KO CD70 nanoCAR T cells, we aimed to evaluate whether MGAT5 KO CD70 nanoCAR T cells are also capable of clearing a tumor upon adoptive transfer *in vivo.*

bioRxiv preprint doi: https://doi.org/10.1101/2023.01.23.525164; this version posted January 23, 2023. The copyright holder for this preprint (which was not certified by peer review) is the author/funder, who has granted bioRxiv a license to display the preprint in perpetuity. It is made available under aCC-BY-NC-ND 4.0 International license.

The NOD.SCID IL2rγ^{null} (NSG) mouse strain has been widely used in the pre-clinical evaluation of CAR T cell efficacy. Immune-deficient NSG mice lack functional mouse T cells, B cells, NK cells and are deficient in cytokine signaling through the common γC receptor[21]. Human tumor xenograft models were established in NSG mice by subcutaneous injection of luciferase-expressing SKOV-3 cells in the flank. Ten days after tumor cell inoculation, the presence of a subcutaneous tumor was evaluated by measurement with a slide caliper and through bioluminescent imaging (BLI) performed using an *in vivo* imaging system (IVIS).

After establishment of a solid, palpable tumor, mice were treated with either mock Cas9-engineered or MGAT5 KO CD70 nanoCAR respectively. As control groups, mice were treated with PBS to evaluate tumor development, or with non-transduced T cells (NTC) to evaluate graft versus host disease (GvHD) and non-specific anti-tumor effects. Throughout the experiment, tumor burden was measured every two days with a caliper and every 4 days through IVIS. A schematic representation of the experimental timeline is depicted in **Figure 3**.A.

At day 34, after the first phase of the experiment, the presence and phenotype of CAR T cells was evaluated in the blood and spleen. Furthermore, mice were followed-up in time and challenged between day 87 and day 90 with a second tumor to evaluate long-term anti-tumor efficacy. Again, tumor burden was evaluated over time and the mice were sacrificed between day 118 and day 123 for end-point analyses.

In the following sections, we will describe the results obtained for two independent experiments (Experiment A and Experiment B), which were performed with T cells from different donors. For the analysis, the treatment groups were divided in three treatment groups of interest: The 'No CAR' group contains the data from all the mice that did not receive any CD70 nanoCAR T cells, and thus includes untreated mice and mice treated with PBS or NTC. The 'CAR' group contains the data from all the mice that received a CD70 nanoCAR T cell treatment, with or without mock Cas9 engineering. The 'CD70 nanoCAR - MGAT5 KO' group contains data from the mice that received MGAT5 knockout CD70 nanoCAR T cells.

The outcome of the treatment was defined by 4 subtypes for the **primary tumor** challenge. (1) Full control meaning the tumor becomes undetectable and no relapse follows. (2) Full control but occurrence of a relapse later on. (3) Partial control meaning a halt in tumor growth but the tumor remains detectable and all mice also experience a relapse after long-term follow-up. (4) No control of tumor growth throughout the duration of the experiment.

As is clear from **Figure 3**.B and the table in **Figure 3**.C, the primary tumor is not controlled by the mice that did not receive CAR T cells, meaning that they were all sacrificed at the humane end-point. When we compare CD70 nanoCAR treated groups with MGAT5 KO CD70 nanoCAR treated groups, we see that more mice control tumor growth when they were treated with MGAT5 KO CD70 nanoCAR T cells, and that all of

bioRxiv preprint doi: https://doi.org/10.1101/2023.01.23.525164; this version posted January 23, 2023. The copyright holder for this preprint (which was not certified by peer review) is the author/funder, who has granted bioRxiv a license to display the preprint in perpetuity. It is made available under aCC-BY-NC-ND 4.0 International license.

these mice show full control, with or without relapse, of primary tumor growth. Contrary to this, a considerable number of mice in the CAR treated group show only partial or even no control at all of the primary tumor.

As opposed to experiment A, in which we did not observe any relapse of the primary tumor over time, the tumor did regrow in some of the treated mice in experiment B. A survival analysis was performed to evaluate whether a difference could be observed in either the number of relapses and the time of their onset between CD70 nanoCAR and MGAT5 KO CD70 nanoCAR T cell treated mice in experiment B (Supplementary Figure 3). When we look at the Kaplan-Meier curves, we indeed observe a difference. The CD70 nanoCAR group seems to have more relapses with an earlier onset in time, leading to a shorter median tumor free survival time of 55 days as compared to the MGAT5 KO CD70 nanoCAR treated group in which the median tumor free survival time is 72 days.

For the secondary tumor, we defined three types of tumor control as no relapse of tumor growth was observed in any of the mice that cleared the secondary tumor. (1) Full control meaning the tumor never develops or becomes undetectable after an initial growth phase. (2) Partial control meaning the tumor stops growing but remains detectable. (3) No control of tumor growth throughout the duration of the experiment.

As is clear from Figure 3.B and the table in Figure 3.D, MGAT5 knockout CD70 nanoCAR T cell treatment also lead to better tumor control after a secondary challenge. While the majority of the mice show no or only partial control of the secondary tumor in the CAR treated groups (52.9% in total), this image is shifted in the MGAT5 KO CAR treated groups (35% in total). In the latter, the majority of the mice completely clear the tumor before the end of the experiment (64% of the mice in total). In the mice that did not clear the secondary tumor completely, the majority of mice treated with the MGAT5 knockout CD70 nanoCAR T cells experienced partial control (21%) while the majority of mice treated with wild type CD70 nanoCAR T cells showed no control at all (47%).

Treatment of tumor-bearing mice with MGAT5 KO CAR T cells leads to a better control of tumor growth rate

To evaluate differences in tumor growth or resolution between the treated mice, a piecewise linear mixed model (with interactions) was fitted (see Supplementary Figure 4 to Supplementary Figure 8) that allows to model the mean tumor volumes in each group. For these analyses, we made a distinction between Experiment A and Experiment B. The main reason for this is that the model would become unnecessarily complex because the timescales (design) of both experiments differ slightly as do the times at which the mice start to respond to the CAR T cell therapy. The latter is possibly due to inherent differences between the CAR T-cell batches (i.e. a donor effect).

bioRxiv preprint doi: https://doi.org/10.1101/2023.01.23.525164; this version posted January 23, 2023. The copyright holder for this preprint (which was not certified by peer review) is the author/funder, who has granted bioRxiv a license to display the preprint in perpetuity. It is made available under aCC-BY-NC-ND 4.0 International license.

In experiment A, we did not observe a difference in the speed of primary tumor resolution in mice treated with CD70 nanoCAR T cells and those treated with MGAT5 KO CD70 nanoCAR T cells (**Supplementary Figure 4**). As even non-glyco-engineered CAR T cells already cleared the primary tumor in a very short time span, there was not much scope for improvement. However, when we look at the response to treatment in the secondary tumor (**Supplementary Figure 5**), differences were observed. While the secondary tumor in the untreated mice grows at 12% (95% CI +9% to +16%) per day (which is consistent with the primary tumor growth), the average growth rate in the CD70 nanoCAR T cell treated group is slower, only 3% per day (95% CI: -15% to +26%). When we look at the MGAT5 KO CD70 nanoCAR T cell treated group, the secondary tumor actually decreases with 10% (95% CI: -24% to +7%) each day, indicating that MGAT5 KO CD70 nanoCAR T cells control tumor growth more efficiently in the secondary phase. However, due to the highly variable responses of individual mice in these groups, the difference in tumor growth rate between the MGAT5 KO CD70 nanoCAR T cell and nanoCAR T cell treated groups is therefore not statistically significant (ratio of growth rates: 95% CI = 0.67 to 1.13, adj. p-value = 0.505).

In experiment B, we do observe a difference in primary tumor clearance when we compare CD70 nanoCAR T cell treated mice with those that received MGAT5 KO CD70 nanoCAR T cells (**Supplementary Figure 6**). The primary tumor loses about half of its volume (49% with 95% CI: -53% to -45%) each day between day 22 and 33 compared to 29% (95% CI: -41% to -24%) each day for the CD70 nanoCAR T cell group. This difference is statistically significant (tumor shrinkage rate in CD70 nanoCAR T cell treated group is only 72% of shrinkage rate in MGAT5 KO CD70 nanoCAR T cell treated group with a 95% CI of 0.59 to 0.86, adj. p-value <0.001). Moreover, while the primary tumor completely disappears in all mice in the MGAT5 KO CD70 nanoCAR T cell treated group in the subsequent part of the experiment (day 33 to about day 84), this is not the case for the CD70 nanoCAR cell treated group, where the tumor volume remaining at day 60 is 5.07 mm^3 (95% CI: 0.32 to 80.07) on average. The confidence interval is quite wide, probably due to the large spread in the CD70 nanoCAR T cell treated group, were some mice clear the tumor completely, some partially and some not at all. Unlike what was observed in experiment A, some of the primary tumors did regrow in the course of the experiment B. From the analysis of these relapsed primary tumors shown in **Supplementary Figure 7**, it is clear that, although the tumor growth rate is the same, the tumor volume is significantly lower in the MGAT5 KO CD70 nanoCAR T cell treated group, as compared to the CD70 nanoCAR T cell treated mice.

The response of CD70 nanoCAR T cell therapy on a secondary tumor challenge in experiment B is summarized in **Supplementary Figure 8**. From day 101 onwards, we see that the tumor size in the MGAT5 KO CD70 nanoCAR T cell treated group decreases with 10% each day (95% CI: -34% to +23%) , while the tumor size in the untreated and CD70 nanoCAR T cell treated groups increases with 9% (95% CI: +1% to +19%) and 6% (95% CI: -10% to +25%) daily respectively, again indicating that MGAT5 KO CD70 nanoCAR

bioRxiv preprint doi: https://doi.org/10.1101/2023.01.23.525164; this version posted January 23, 2023. The copyright holder for this preprint (which was not certified by peer review) is the author/funder, who has granted bioRxiv a license to display the preprint in perpetuity. It is made available under aCC-BY-NC-ND 4.0 International license.

T cells lead to a better tumor control after a secondary challenge. However, the difference in growth rate between CD70 nanoCAR T cell treated mice and MGAT5 KO CD70 nanoCAR T cell treated mice is not statistically significant (growth speed in MGAT5 KO CD70 nanoCAR T treated mice is 0.85 times the growth rate in CD70 nanoCAR T cell treated mice, 95% CI 0.59 to 1.22). This is most probably due to the large variability and relatively few available mice within the treatment groups.

MGAT5 KO CD70 nanoCAR T cells are present in higher numbers than CD70 nanoCAR T in peripheral blood and spleen following tumor control

End-point analysis on day 34 was performed on peripheral blood (both experiments) and spleen (experiment A) by flow-cytometry (**Figure 4**-A,B,F). Human $CD3^+$ T cells were detected in blood and spleen of mice treated with mock Cas9 or MGAT5 KO CD70 nanoCAR T cells and around 75% of these cells were found to be CD70 nanoCAR T cells (data not shown), based on GFP expression. The number of MGAT5 KO CD70 nanoCAR T cells in the spleen (**Figure 4**-B) and blood (**Figure 4**-F) is markedly increased as compared to mock Cas9 CD70 nanoCAR T cells. We did not analyze splenocytes on day 34 in experiment B, since we kept all mice for rechallenge, enabling statistics on larger groups. CAR T cells were still present in the blood at day 80 (**Figure 4**-C,G). We see a trend of higher numbers of MGAT5 KO CD70 nanoCAR T cells compared to CD70 nanoCAR T cells, mostly pronounced in experiment B, however, the difference is not statistically significant. End-point analysis between day 118 and day 123 was performed on peripheral blood and spleen (**Figure 4**-E,I). Similarly, in both experiments we measure higher numbers of MGAT5 KO CD70 nanoCAR T cells compared to CD70 nanoCAR T cells, however, the difference is not statistically significant.

Discussion

In this paper, we described the impact of cell surface glycosylation alterations on T cell fate and functions through MGAT5 KO induced in CD70 nanoCAR T cells. As the alteration of cellular glycosylation has an impact on multiple cell surface receptors and their signal transduction, we measured the integrated results of all of these alterations on cellular behavior, both *in vitro* and *in vivo.*

β1,6-N-acetylglucosaminyltransferase-V (MGAT5) is the enzyme responsible for the initiation of GlcNAc-β-(1,6)-branching on N-glycans and is involved in multiple aspects of T cell activation. β-(1,6)-N-glycan branching leads to an increase in LacNAc modifications, the ligand of Galectins. It has been demonstrated that absence of *Mgat5* and thus a decrease in LacNAc, lowers T cell activation thresholds *in vitro* by enhancing TCR clustering due to the absence of Galectin-glycoprotein lattice formation[22,23]. This Galectin-mediated lattice is responsible for holding CD45 and the TCR signaling complex in close proximity via their O- and N-linked glycans (respectively) to prevent low-avidity T cell activation[24]. Greco *et al.* recently demonstrated, by knockout of *Mgat5* in pancreatic adenocarcinoma, that N-glycans protect tumors from CAR T cell killing by interfering with proper immunological synapse formation and reducing transcriptional

bioRxiv preprint doi: https://doi.org/10.1101/2023.01.23.525164; this version posted January 23, 2023. The copyright holder for this preprint (which was not certified by peer review) is the author/funder, who has granted bioRxiv a license to display the preprint in perpetuity. It is made available under aCC-BY-NC-ND 4.0 International license.

activation, cytokine production and cytotoxicity[25]. It is known MGAT5 is a primary target of the Golgi-resident intramembrane protease Signal peptide peptidase-like 3 (SPPL3)[26]. Along the same line as described by Greco *et al.*, Heard and colleagues identified expression of SPPL3 in malignant B cells as a potent regulator of resistance to CAR therapy [27].

An increased incidence of autoimmune disease is seen in the absence of *Mgat5 in vivo*[19]. Furthermore, negative regulation of TCR signaling by β1,6-GlcNAc-containing *N*-glycans promotes development of Th2 over Th1 responses, enhances Th2 polarization, and suggests a mechanism for the increased autoimmune disease susceptibility observed in *Mgat5*$^{-/-}$ mice[28]. On the other hand, *Mgat5* expression can be induced by the anti-inflammatory cytokine IL-10, decreasing antigen sensitivity of CD8^{+} T cells during chronic infection[29].

Our results indicate that MGAT5 KO CD70 nanoCAR T and CD70 nanoCAR T largely behave in the same way as control cells *in vitro*; MGAT5 elimination had no clear impact on T cell activation or viability. Furthermore, anti-tumor cell responses by MGAT5 KO CD70 nanoCAR T cells were maintained *in vitro* and very interestingly, our results indicate that MGAT5 KO nanoCAR T cells show enhanced anti-tumor potential and control upon a primary and secondary tumor challenge, as compared to mock engineered CAR T cells. In the case of very potent CAR T cells (cfr in experiment A), the improved protective effect of MGAT5 KO CD70 nanoCAR T cells over CD70 nanoCAR T cells seems to be more pronounced upon rechallenge, however, when CAR T cells are less potent (cfr in experiment B), enhanced capability seems to be more explicit in clearance of the primary tumor. Notably, increased numbers of MGAT5 KO CD70 nanoCAR T cells were observed upon specific antigen recognition, both *in vitro* and *in vivo.*

It was previously shown that the inhibition of binding to LacNAc glycans via competitive inhibition with carbohydrate analogs increased the number of infiltrating tumor-specific T cells[30]. In a recent study by Ye *et al.*[31], MGAT5 was discovered as one of the top hits in a CRISPR screen in murine CD8^{+} T cells in a syngeneic model of glioblastoma in immunocompetent mice. MGAT5 knockout enhanced the efficacy of adoptive T cell transfer against glioblastoma in mice with both immunocompetent and antigen-specific transgenic TCR models in terms of increased tumor infiltration and overall survival of tumor bearing mice.

A possible explanation for the higher numbers of MGAT5 KO CD70 nanoCAR T cells compared to control CD70 nanoCAR T cells, could be that MGAT5 KO CAR T cells are less susceptible to Galectin-3-mediated apoptosis. We already confirmed Galectin-3 overexpression by the tumor cell lines used in our models and we are currently evaluating whether Galectin-3 binding to MGAT5 KO (CAR) T cells is indeed reduced. To capture the transcriptional programs that are differentially regulated between glyco-engineered and wild type CAR T cells, we will perform transcriptome profiling by bulk mRNA sequencing on cells that are cultured in the absence and presence of antigen expressing cells. Gene set enrichment and pathway

bioRxiv preprint doi: https://doi.org/10.1101/2023.01.23.525164; this version posted January 23, 2023. The copyright holder for this preprint (which was not certified by peer review) is the author/funder, who has granted bioRxiv a license to display the preprint in perpetuity. It is made available under aCC-BY-NC-ND 4.0 International license.

370 analyses can then reveal a signature of gene upregulation or downregulation specific to knockout cell
371 populations[32]. Results of this experiment are expected soon.

372 Taken together, it is clear from our data that disruption of N-glycosylation modifications on CAR T cells can
373 have a major impact on their antitumor efficacy, and thus might have important implications for future
374 design of cell-based immunotherapies.

375 # Materials and methods

376 ## Ethical approval

377 All experiments were approved and performed according to the guidelines of the ethical committee
378 Medical Ethics of Ghent University, Belgium.

379 The breeding of NSG mice is covered by file E-726 and animal experiments are covered by file EC2020-009.

380 ## Cell lines

381 THP-1 cells were obtained from ATCC and cultured in RPMI medium (Gibco) supplemented with 10% fetal
382 calf serum (FCS), 0.03% L-Gln, 0.4 mM sodium pyruvate and 50 µM β-mercaptoethanol. SKOV-3 cells
383 expressing luciferase were kindly provided by Prof. De Wever (Ghent University, Faculty of Medicine and
384 Health Sciences) and were cultured in DMEM medium (Gibco) supplemented with 10% FCS and 1%
385 penicillin/streptomycin. Jurkat cells were obtained from ATCC and were cultured in RPMI medium (Gibco)
386 supplemented with 10% FCS, 2mM L-Gln and 0.4 mM sodium pyruvate. All cell lines were maintained in a
387 37°C, 5% CO_2, fully humidified incubator and passaged twice weekly.

388 ## Human $CD3^+$ T cell isolation and culturing

389 Leukocyte-enriched buffy coat samples were obtained from healthy donors attending the Red Cross center
390 after informed consent and ethical committee approval (EC2019-1083). Peripheral blood lymphocytes
391 were prepared by a Ficoll-Paque density centrifugation as described in the instruction manual for
392 Leucosep™ (Greiner bio-one). $CD3^+$ T cells were isolated by negative selection with antibodies against
393 CD14, CD15, CD16, CD19, CD36, CD56, CD123 and CD235 (MojoSort™ Human CD3 T cell selection kit,
394 Biolegend) according to the manufacturer's protocol. Cells were cultured in IMDM + Glutamax medium
395 (Gibco-BRL) supplemented with 10% heat-inactivated FCS and stimulated with Immunocult™ Human
396 CD3/CD28 T cell Activator (Stemcell Technologies) (25 µL/ 10^6 cells) for 3 days at 37°C in the presence of
397 10 ng/ mL IL-12 (Biolegend).

398 Prior to cell seeding, cells were washed twice with PBS before putting them in culture with rhIL-7 at
399 10ng/mL (Miltenyi) and rhIL-15 at 10 ng/mL (Miltenyi). Cytokines and medium were replaced every 2-3
400 days. Cell densities were maintained between 1 x 10^6 and 3 x 10^6 cells/ mL.

bioRxiv preprint doi: https://doi.org/10.1101/2023.01.23.525164; this version posted January 23, 2023. The copyright holder for this preprint (which was not certified by peer review) is the author/funder, who has granted bioRxiv a license to display the preprint in perpetuity. It is made available under aCC-BY-NC-ND 4.0 International license.

Guide RNA

We designed gRNAs using the Synthego design tool (https://www.synthego.com/products/bioinformatics/crispr-design-tool). Guides were ordered as chemically modified synthetic sgRNAs (with 2'O-Methyl at 3 first and 3 last bases and 3' phosphorothioate bonds between first 3 and last 2 bases) and reconstituted at 100 µM in TE buffer. An overview of the guides used in this study can be consulted in **Supplementary Figure 2.**A.

RNP electroporation

Recombinant Cas9-GFP protein was purchased from the VIB protein core (https://vib.be/labs/vib-protein-core). Cas9 RNP was made by incubating Cas9 protein with sgRNA at a molar ratio of 1:2 at 37°C for 15 min immediately prior to electroporation in T cells. Electroporation was performed using the Lonza Amaxa 4D Nucleofector X unit (Program EH-115) and the P3 primary cell kit with the following conditions: 1 x 10^6 cells/20 µL P3 buffer per cuvette (16-well strips) with 20 µM Cas9-RNP. Following nucleofection, 80 µL pre-warmed medium was added per well and cells were allowed to rest for 30 mins at 37°C, 5% CO_2.

Analysis of genome editing efficiency

0.1 x 10^6 cells were collected and lysed in QuickExtract™ (Lucigen Epicentre) according to the supplier's instructions. The target site was amplified by PCR and Sanger Sequenced. Sequencing data was analyzed with the ICE tool (Inference of CRISPR Edits, Synthego) to infer the percentage of insertions and deletions (INDEL score) and the percentage of insertions and deletions that are out of frame (knock out (KO) score)[33].

Production of retroviral vectors

Retroviral constructs encoding the nanoCAR sequences were previously cloned in the LZRS-IRES-eGFP vector and were obtained from Prof. Dr. Bart Vandekerckhove (Department of Diagnostic Sciences, Ghent University, 9000 Ghent, Belgium). Viral particles were produced using standard $Ca_3(PO_4)_2$ transfection of the Phoenix ampho packaging cell line. Retroviral supernatant was collected at day 14 after transfection and puromycin selection and kept at -80°C until use.

Generation of CD70 nanoCAR Expressing Human T cells

Immunocult-stimulated human $CD3^+$ T cells were retrovirally transduced on Retronectin-coated plates (TaKaRa). 500 µL of cells per well at 0.5 x 10^6 cells/mL were supplemented with 0.5 mL retroviral supernatant and centrifuged for 90 minutes at 900 g at 32°C. Transduced cells were detected by eGFP expression or by an anti-VHH antibody (Genscript) directed against the nanobody constituting the extracellular domain of the CAR and analyzed by flow cytometry.

bioRxiv preprint doi: https://doi.org/10.1101/2023.01.23.525164; this version posted January 23, 2023. The copyright holder for this preprint (which was not certified by peer review) is the author/funder, who has granted bioRxiv a license to display the preprint in perpetuity. It is made available under aCC-BY-NC-ND 4.0 International license.

Lectin-based flow cytometry

For the evaluation of the poly-LacNAc content on the cell surface, we used the lectin from *Datura stramonium* at a staining concentration of 10 µg/ mL (Biotinylated DSL, Vector laboratories, B-1185-2). 2 x 10^5 cells per condition were collected and rinsed three times with PBS. Cells were incubated with fixable viability dye eFl780 (eBioscience) and biotinylated lectin in lectin binding buffer (PBS with 0.1 mM $CaCl_2$) for 30 minutes at 4°C. After rinsing with lectin binding buffer, cells were incubated with PE-coupled neutravidin (Invitrogen, 5 µg/mL) for 30 minutes at 4°C. After rinsing the cells with PBS, samples were resuspended and analyzed by flow cytometry. A minimum of 50 000 events was recorded.

PNGaseF digest

In order to prepare cell surface N-glycans for DSA-FACE analysis, 1 x 10^6 cells were collected per condition and washed three times with PBS to reduce the presence of medium-derived glycans. Cell culture medium was collected for N-glycan labeling. PNGaseF digest (0.125 IU/ 1x10^6 cells, in-house production) was performed in 25 µL final volume in PBS for 2 hours at 37°C. Cells were removed by centrifugation (5 min at 300g) and the supernatant was subjected to another centrifugation step (15 min at 15 000 rpm) to remove cell debris. The remaining liquid portion of the sample was stored at -20°C until APTS labeling and DSA-FACE analysis.

N-glycan analysis using DSA-FACE

The remaining N-glycan samples were labelled by adding an equal volume (20 µL) of labeling mix consisting of a 1/1 v/v mix of 1M morpholine borane in 20% DMSO, 20% SDS and 4M Urea mixed with 350 mM APTS in 2.4M citric acid and 14% SDS immediately prior to labeling. The labeling reaction was incubated at 70°C for 1 hour and allowed to cool down at 4°C before purification. Size exclusion chromatography (Sephadex G-10 resin with an exclusion limit of 700 Da prepared in a 96-well setup in Multiscreen-Durapore plates) was performed twice to desalt the samples and to remove free unreacted APTS[34]. The labeled glycans were then dried in a speedvac.

Purified labelled and dried N-glycans were resuspended in 10 µL ultrapure water and analyzed with capillary electrophoresis on an eight-capillary DNA sequencer (Applied Biosystems 3500 Genetic analyzer). A proprietary internal standard (GlyXera) was added to the samples to be able to align profiles from different samples. Samples were injected on a 50 cm capillary at 15 kV for 10 seconds, using POP7 polymer and 100 mM TAPS, pH 8,0, containing 1 mM EDTA as the running buffer. N-glycan profiles were analyzed through the Genemapper 6 software.

bioRxiv preprint doi: https://doi.org/10.1101/2023.01.23.525164; this version posted January 23, 2023. The copyright holder for this preprint (which was not certified by peer review) is the author/funder, who has granted bioRxiv a license to display the preprint in perpetuity. It is made available under aCC-BY-NC-ND 4.0 International license.

Flow cytometry analysis

Flow cytometry analysis was performed on 0.2 x 10^6 cells per sample collected in a 96-well V bottom plate. Cells were rinsed with FACS buffer (PBS containing 0.5% BSA and 2mM EDTA) for 3 min at 300g and incubated with Fc Receptor Blocking solution (Human TruStain FcX™, Biolegend) for 10 minutes prior to cell surface staining with fluorescently labeled antibodies in Brilliant Stain buffer (BD Biosciences) for 30 minutes at 4°C.

For human $CD3^+$ T cell phenotyping, cells were labeled with fluorescent antibodies against human CD8, CD62L and CD45RA (BD Biosciences) and CD3, CD4, CD25, CD69, and CD279 (PD-1) (Biolegend). A Fixable dye eFluor™ 780 (eBioscience) was used to evaluate live/dead cells.

Flow cytometer calibration was performed using CS&T beads (BD Biosciences). The gating strategy was set based on fluorescence minus one (FMO) controls and retained for all samples. Jurkat, THP-1 and SKOV-3 cell lines and primary human T cells were labeled with fluorescent antibody against human CD70 or isotype control (Biolegend) to verify antigen expression as described before[35].

Galectin expression by tumor cell lines was evaluated by cell surface staining with a fluorescent antibody against Galectin-3 and an antibody against Galectin-1. The latter was detected by a fluorescent anti-goat antibody. As a positive control, cells were incubated with 200 µg/mL recombinant Galectin-1 and Galectin-3 (Biolegend). Galectin binding was competitively inhibited by adding 50 mM lactose during the staining procedure.

In all analyses, following doublet exclusion, live cells were identified using a fixable viability dye (Molecular Probes, Life Technologies). Data were acquired on a BD Symphony A5 equipped with five lasers (355, 405, 488, 561, 640nm) (BD Biosciences) and analyzed using FlowJo software (Tree Star, Ashland, OR).

In vitro analysis of cytokine production

Glyco-engineered CD70 nanoCAR T cells were stimulated *in vitro* by co-incubation with THP-1 or SKOV-3 tumor cell lines expressing CD70 in a 96-well plate in duplicate. After 1 hour of co-incubation, BD GolgiPlug (BD Biosciences) was added and after an additional 15 hours of stimulation, the cells were harvested, labelled with fluorescent antibodies against CD3, CD4 and CD8, fixed and permeabilized (eBioscience) and labelled for intracellular expression cytokines with fluorescent antibodies against TNF-α (BD Biosciences), IFN-γ and IL-2 (Biolegend). Samples were analyzed by flow cytometry as described above.

bioRxiv preprint doi: https://doi.org/10.1101/2023.01.23.525164; this version posted January 23, 2023. The copyright holder for this preprint (which was not certified by peer review) is the author/funder, who has granted bioRxiv a license to display the preprint in perpetuity. It is made available under aCC-BY-NC-ND 4.0 International license.

In vitro analysis of tumor cell killing

Glyco-engineered CD70 nanoCAR T cells were incubated with 2 x 10^4 THP-1 cells at different effector/target ratios (0; 0.0015; 0.015 and 0.15) in IMDM medium with Glutamax (Gibco) containing 10% FCS and 1% penicillin/streptomycin. Cells were labelled with fluorescent antibodies against CD3, CD4 and CD8 for the analysis of T cells and CD33 for the analysis of THP-1 cells at the start of the co-culture (day 0) and at day 3, 7, 10 and 14. At day 7 of co-culture, 2 x 10^4 THP-1 cells were added to the remaining wells. Cell numbers were determined by flow cytometry.

In vivo analysis of glyco-engineered CD70 nanoCAR T cell efficacy

NSG mice (breeder pairs obtained from The Jackson Laboratory, breeding in house) between 8-12 weeks of age were subcutaneously (in the flank) injected with 2 x 10^6 SKOV-3 cells in 50 µL PBS. The cells were allowed to form a solid mass tumor and CD70 nanoCAR T cells were intravenously injected on day 13 (in 200 µL total volume in PBS). Body weight and tumor progression was followed up by caliper and bioluminescence imaging (BLI). A dose of 150 mg/kg D-luciferin potassium salt (Perkin Elmer) was injected intraperitoneally 10 minutes before BLI. Imaging data were analyzed using Living Image Software and reported as photons/second. In experiment A, we started with 6 mice in the PBS and NTC group and 12 mice in the CD70 nanoCAR mock Cas9/MGAT5KO groups. At day 34, all control mice and 6 mice from the CD70 nanoCAR mock Cas9/MGAT5KO groups were sacrificed for analysis. The other 6 mice from the CD70 nanoCAR mock Cas9/MGAT5KO groups were kept for rechallenge. In experiment B, we started with 6 mice in the PBS and NTC group and 9 mice in the CD70 nanoCAR mock Cas9/MGAT5KO groups. All mice were kept for rechallenge, unless humane endpoint was reached (control mice). At the start of each experiment, we also kept a group of 8 (experiment A) or 6 (experiment B) mice to be used as a control (=PBS) group in the rechallenge phase of the experiment, to ensure age-matched controls.

End-point analysis on spleen and blood

At indicated time points, mice were euthanized. Peripheral blood was collected following severing of the right atrium of the heart and transferred to EDTA coated Microvettes (Sarstedt). The volume of blood was determined and red blood cells were removed using ammonium-chloride-potassium (ACK) lysis buffer (Lonza) prior to antibody staining for flow cytometry analysis.

The spleen was collected and processed to a cell suspension through a 70 µM cell strainer. Erythrocytes were removed using ACK lysis buffer followed by washes. Cells were counted prior to antibody staining for flow cytometry analysis.

Tumors were isolated from non-treated controls and fixed in 4% PFA. Subsequently, tumor tissue was embedded in paraffin for downstream immunohistochemistry analysis.

bioRxiv preprint doi: https://doi.org/10.1101/2023.01.23.525164; this version posted January 23, 2023. The copyright holder for this preprint (which was not certified by peer review) is the author/funder, who has granted bioRxiv a license to display the preprint in perpetuity. It is made available under aCC-BY-NC-ND 4.0 International license.

Immunohistochemistry and microscopic analysis of galectin expression in tumor tissue

Immunofluorescent staining was performed on 4 µm thick formalin-fixed, paraffin embedded (FFPE) sections of tumor samples from untreated mice. After antigen retrieval using citrate buffer pH 6 (Vector, H-3300), sections were incubated with 1% goat serum in PBS + 0.5% BSA + 0.1% Tween20 for 30 minutes to block non-specific binding. Subsequently, monoclonal rabbit anti-galectin-1 (1:200, Cell Signaling, 13888S) or monoclonal rabbit anti-galectin-3 (1:200, Cell Signaling, 87985S) diluted in 1% w/v goat serum in PBS + 0.5% BSA + 0.1% Tween20 were incubated at overnight at 4°C. Alexa Fluor 568 labelled goat anti-rabbit (1:500, Thermofisher, A11036), was incubated at room temperature for two hours. Counterstaining was performed using DAPI (1:1000). Slides were mounted using 1% n-propyl-gallate in glycerol (pH7). Images of the galectin staining were acquired with a LSM880 confocal microscope (Zeiss) and analyzed through ZEN Microscopy Software (Zeiss).

Statistical analysis *in vitro* experiments assessing tumor cell killing

To analyze the data of the coculture experiment, we started from flow cytometry-based count data. Since the counts had been normalized using counting beads, they were not necessarily integers so we rounded all to the closest integer. We considered each setup with the same donor, E/T Ratio and type of CAR T cells (i.e. CD70 nanoCAR or CD70 nanoCAR MGAT5 KO) as a cluster. Since we had two measurements (repeats) at each day and the measurements were performed at day 0, 4, 7, 11 and 14, this means we had 10 measurements in each cluster. Furthermore, we observed a slight rise in the counts of the NTC cells over time in the control setups. We corrected the CAR T cell counts for this background (per cluster and at each timepoint) by subtracting the mean background count from the measurements.

We analyzed the background-corrected counts with a generalized linear mixed model (GLMM) to allow for modeling the within-cluster correlation over time. Since the data showed considerable overdispersion, we used a negative binomial model. The GLMMadaptive package[36] allows to fit such a model in R[37] using adaptive Gaussian quadrature (AGQ). We did not have enough data to fit a random slope model, so we settled for a random intercept model of the following form:

$$\text{Count} \sim \text{fDay}*(\text{Group} + \text{Donor} + \text{ETRatio}) + \text{Group}*\text{Donor} + (1|\text{cluster})$$

In this model, all fixed effects are coded as a factor. We chose to also model the time variable as a factor since the log-transformed counts are not linear with time. The model fit was evaluated using the DHARMa package[38] and contrasts were estimated using the multcomp package[39].

Statistical analyses *in vivo* experiments

Multinomial logistic regression

We analyzed the distributions of outcomes for the primary and secondary tumors in the different groups of mice. To do so, we first had to define several possible outcomes. For the primary tumor, there are four

bioRxiv preprint doi: https://doi.org/10.1101/2023.01.23.525164; this version posted January 23, 2023. The copyright holder for this preprint (which was not certified by peer review) is the author/funder, who has granted bioRxiv a license to display the preprint in perpetuity. It is made available under aCC-BY-NC-ND 4.0 International license.

possible outcomes: - Full control of the tumor, meaning that the tumor becomes undetectable both by caliper measurement and on BLI, and also no relapse. - Full control of the tumor but with a relapse after a period of the tumor being undetectable. - Partial control, meaning that the tumor stops growing but remains detectable, all these mice also had a relapse. - No control of tumor meaning that the tumor continually keeps growing. For the secondary tumor we only have full control, partial control or no control. The follow up time was not long enough to also consider relapses. To analyze these data in R[37], we used multinomial logistic regression (with a proportional odds assumption) as implemented in the polr function of the MASS package[40]. We analyzed the outcomes of experiments A and B together making experiment an additional predictor apart from group. Using likelihood ratio testing, we tested for an interaction effect between experiment and group and found that this was not significant in the primary nor secondary tumor. We used the multcomp package[39] to calculate contrast estimates with 95% confidence intervals. We also used the ggpredict function from the ggeffects package[41] to calculate experiment-wise predictions with 95% confidence intervals for the predicted outcomes.

Survival analysis (time to relapse)

To analyze the time to relapse, we first defined the start of follow up as the moment the primary tumor was controlled or partially controlled. We define control as the first day the tumor became completely undetectable on BLI and by caliper measurement. We define partial control as the first day a tumor (that never fully disappears) stopped increasing in size according to caliper measurements. Next, we define a relapse event as the moment a tumor starts growing again. We take the last day before the tumor has increased in size again or became detectable again as the onset of relapse. The time to event is then the time between start of follow up and a relapse event and the follow up time is the time between start of follow up and either an event or the end of follow up in case of no relapse. We used R[37] with the survival[42,43] and survminer[44] packages to generate Kaplan-Meier plots with estimates of the median survival times and a corresponding risk and events table. Since relapses were only observed in experiment B, we ran a straightforward analysis with group as the only predictor (groups: CD70 nanoCAR or CD70 nanoCAR - MGAT5 KO). We tested for the difference in survival probability in these groups with a logrank test as implemented in the survival package.

Longitudinal analyses

Tumor volumes were measured by measuring the length and width of a tumor and using the length* width*width/2 (this is a half cube or cuboid) approximation of the volume of a sphere. The smallest tumor length/width that can be reliably measured with a caliper is about 0.5 cm. The minimal tumor volume that can be calculated in this way is 0.5*0.5*0.5/2 = 0.0625 cm^3 (which can be regarded as the limit of quantification). We also cross-checked with BLI data for the small tumors, since this gives a better indication on whether there actually is still a tumor present or not. Whenever a small tumor was measured

bioRxiv preprint doi: https://doi.org/10.1101/2023.01.23.525164; this version posted January 23, 2023. The copyright holder for this preprint (which was not certified by peer review) is the author/funder, who has granted bioRxiv a license to display the preprint in perpetuity. It is made available under aCC-BY-NC-ND 4.0 International license.

or a zero volume was registered, BLI was used to verify whether a tumor was actually present or not and the caliper measurements were adapted accordingly: when no tumor was found on BLI, we set small caliper measurements to zero and when a tumor was found on BLI but not measured by caliper, we set the tumor volume to 0.5. Uncontrolled tumor growth is exponential so we log-transformed (with a base 2 log) all tumor volume data to simplify the mean structures of the fitted models and to correct for the mean-variance relationship we observed during data exploration. To avoid problems when the tumor volume is zero, we first added 0.0625 (the detection limit) to all volumes before log-transforming. We then analyzed the transformed data of each experiment (A and B) and each phase (primary tumor before and after rechallenge and secondary tumor) separately by fitting a linear mixed model to each using the lme4 package[45] and the nlminb fitting algorithm from the optimx package[46] in R[37]. Where needed, we used piece-wise linear models with up to two knots for the time variable to allow for changes in growth rate over time. Random effects included a per-mouse random intercept and one or more random slopes for the time variable to model within-mouse correlation over time. For each model, we started with mean and covariance structures that were as saturated as possible based on the available data. Pruning the models was done via likelihood ratio testing first using Residual maximum likelihood (REML) to test for the random effects and then maximum likelihood (ML) to test for fixed effects. The final models were fitted using REML. In all models, we observed residual heteroscedasticity, even with the log-transformed data, so we used robust covariance estimators from the clubSandwich package[47] (vcovCR, type 'CR0') in conjunction with the multcomp package[39] to calculate adjusted p-values and/or adjusted 95% confidence intervals for parameters and contrasts.

Acknowledgements

NF and LM were staff scientists of VIB. EDB was a predoctoral fellow at FWO during the project and has currently a doctor-assistant mandate at UGhent. EP was a research associate of VIB, AVH and EW are research associates of UGhent. This work was supported by grants G050420N and G028220N of FWO Vlaanderen and by a Young Investigator Proof of Concept (YIPOC) grant of the Cancer Research Institute Ghent (CRIG). We are grateful to M. Goossens and L. De Pryck for help with the caliper/IVIS measurements, splenocyte preparations and collecting SKOV3 cells. We thank Prof. Dr. Y. Chen (Parker Institute for Cancer Immunotherapy Center at UCLA, Los Angeles, CA, USA) for intensive experimental training in the CAR T field. We thank the VIB Bioimaging core Ghent (https://vib.be/labs/vib-bioimaging-core-ghent) and VIB Flow Core (https://vib.be/labs/vib-flow-core-ghent) facilities for their services.

bioRxiv preprint doi: https://doi.org/10.1101/2023.01.23.525164; this version posted January 23, 2023. The copyright holder for this preprint (which was not certified by peer review) is the author/funder, who has granted bioRxiv a license to display the preprint in perpetuity. It is made available under aCC-BY-NC-ND 4.0 International license.

Declaration of interest statement

EDB, NF and NC are co-inventors on a PCT International Patent application (PCT/EP2022/086474) by the VIB and Ghent University, which incorporate discoveries and inventions described here. All the other authors declare no conflict of interest.

References

1. De Bousser E, Callewaert N, Festjens N. T Cell Engaging Immunotherapies, Highlighting Chimeric Antigen Receptor (CAR) T Cell Therapy. Cancers 2021; 13:6067.

2. Vairy S, Garcia JL, Teira P, Bittencourt H. CTL019 (tisagenlecleucel): CAR-T therapy for relapsed and refractory B-cell acute lymphoblastic leukemia. Drug Des Devel Ther 2018; 12:3885–98.

3. Reagan PM, Friedberg JW. Axicabtagene ciloleucel and brexucabtagene autoleucel in relapsed and refractory diffuse large B-cell and mantle cell lymphomas. Future Oncol Lond Engl 2021; 17:1269–83.

4. Liu L, Qu Y, Cheng L, Yoon CW, He P, Monther A, Guo T, Chittle S, Wang Y. Engineering chimeric antigen receptor T cells for solid tumour therapy. Clin Transl Med 2022; 12:e1141.

5. De Bousser E, Meuris L, Callewaert N, Festjens N. Human T cell glycosylation and implications on immune therapy for cancer. Hum Vaccines Immunother 2020; 16:2374–88.

6. Okada M, Chikuma S, Kondo T, Hibino S, Machiyama H, Yokosuka T, Nakano M, Yoshimura A. Blockage of Core Fucosylation Reduces Cell-Surface Expression of PD-1 and Promotes Anti-tumor Immune Responses of T Cells. Cell Rep 2017; 20:1017–28.

7. Alegre ML, Frauwirth KA, Thompson CB. T-cell regulation by CD28 and CTLA-4. Nat Rev Immunol 2001; 1:220–8.

8. Lau KS, Partridge EA, Grigorian A, Silvescu CI, Reinhold VN, Demetriou M, Dennis JW. Complex N-Glycan Number and Degree of Branching Cooperate to Regulate Cell Proliferation and Differentiation. Cell 2007; 129:123–34.

9. Demotte N, Wieërs G, Van Der Smissen P, Moser M, Schmidt C, Thielemans K, Squifflet J-L, Weynand B, Carrasco J, Lurquin C, et al. A galectin-3 ligand corrects the impaired function of human CD4 and CD8 tumor-infiltrating lymphocytes and favors tumor rejection in mice. Cancer Res 2010; 70:7476–88.

10. Clemente T, Vieira NJ, Cerliani JP, Adrain C, Luthi A, Dominguez MR, Yon M, Barrence FC, Riul TB, Cummings RD, et al. Proteomic and functional analysis identifies galectin-1 as a novel regulatory component of the cytotoxic granule machinery. Cell Death Dis 2017; 8:e3176.

11. Wang H, Kaur G, Sankin AI, Chen F, Guan F, Zang X. Immune checkpoint blockade and CAR-T cell therapy in hematologic malignancies. J Hematol OncolJ Hematol Oncol 2019; 12:59.

12. Yu F, Finley RL, Raz A, Kim H-RC. Galectin-3 translocates to the perinuclear membranes and inhibits cytochrome c release from the mitochondria. A role for synexin in galectin-3 translocation. J Biol Chem 2002; 277:15819–27.

13. Kouo T, Huang L, Pucsek AB, Cao M, Solt S, Armstrong T, Jaffee E. Galectin-3 shapes antitumor immune responses by suppressing CD8+ T cells via LAG-3 and inhibiting expansion of plasmacytoid dendritic cells. Cancer Immunol Res 2015; 3:412–23.

bioRxiv preprint doi: https://doi.org/10.1101/2023.01.23.525164; this version posted January 23, 2023. The copyright holder for this preprint (which was not certified by peer review) is the author/funder, who has granted bioRxiv a license to display the preprint in perpetuity. It is made available under aCC-BY-NC-ND 4.0 International license.

14. Stillman BN, Hsu DK, Pang M, Brewer CF, Johnson P, Liu F-T, Baum LG. Galectin-3 and galectin-1 bind distinct cell surface glycoprotein receptors to induce T cell death. J Immunol Baltim Md 1950 2006; 176:778–89.

15. Chen H-Y, Fermin A, Vardhana S, Weng I-C, Lo KFR, Chang E-Y, Maverakis E, Yang R-Y, Hsu DK, Dustin ML, et al. Galectin-3 negatively regulates TCR-mediated CD4+ T-cell activation at the immunological synapse. Proc Natl Acad Sci U S A 2009; 106:14496–501.

16. Kaur M, Kumar D, Butty V, Singh S, Esteban A, Fink GR, Ploegh HL, Sehrawat S. Galectin-3 Regulates γ-Herpesvirus Specific CD8 T Cell Immunity. iScience 2018; 9:101–19.

17. Petit A-E, Demotte N, Scheid B, Wildmann C, Bigirimana R, Gordon-Alonso M, Carrasco J, Valitutti S, Godelaine D, van der Bruggen P. A major secretory defect of tumour-infiltrating T lymphocytes due to galectin impairing LFA-1-mediated synapse completion. Nat Commun 2016; 7:12242.

18. Demotte N, Stroobant V, Courtoy PJ, Van Der Smissen P, Colau D, Luescher IF, Hivroz C, Nicaise J, Squifflet JL, Mourad M, et al. Restoring the Association of the T Cell Receptor with CD8 Reverses Anergy in Human Tumor-Infiltrating Lymphocytes. Immunity 2008; 28:414–24.

19. Demetriou M, Granovsky M, Quaggin S, Dennis JW. Negative regulation of T-cell activation and autoimmunity by Mgat5 N-glycosylation. Nature 2001; 409:733–9.

20. De Munter S, Buhl J, De Cock L, Van Parys A, Daneels W, Pascal E, Deseins L, Ingels J, Goetgeluk G, Billiet L, et al. Knocking out CD70 rescues CD70-specific nanoCAR T cells from antigen induced exhaustion. bioRxiv/523482 2023; https://doi.org/10.1101/2023.01.22.523482.

21. Maletzki C, Bock S, Fruh P, Macius K, Witt A, Prall F, Linnebacher M. NSG mice as hosts for oncological precision medicine. Lab Invest 2019; :1–11.

22. Dennis JW, Lau KS, Demetriou M, Nabi IR. Adaptive Regulation at the Cell Surface by N-Glycosylation. Traffic 2009; 10:1569–78.

23. Li D, Li Y, Wu X, Li Q, Yu J, Gen J, Zhang X-L. Knockdown of Mgat5 Inhibits Breast Cancer Cell Growth with Activation of CD4+ T Cells and Macrophages. J Immunol 2008; 180:3158–65.

24. Earl LA, Bi S, Baum LG. N- and O-Glycans Modulate Galectin-1 Binding, CD45 Signaling, and T Cell Death. J Biol Chem 2010; 285:2232–44.

25. Greco B, Malacarne V, De Girardi F, Scotti GM, Manfredi F, Angelino E, Sirini C, Camisa B, Falcone L, Moresco MA, et al. Disrupting N-glycan expression on tumor cells boosts chimeric antigen receptor T cell efficacy against solid malignancies. Sci Transl Med 2022; 14:eabg3072.

26. Voss M, Künzel U, Higel F, Kuhn P-H, Colombo A, Fukumori A, Haug-Kröper M, Klier B, Grammer G, Seidl A, et al. Shedding of glycan-modifying enzymes by signal peptide peptidase-like 3 (SPPL3) regulates cellular N-glycosylation. EMBO J 2014; 33:2890–905.

27. Heard A, Landmann JH, Hansen AR, Papadopolou A, Hsu Y-S, Selli ME, Warrington JM, Lattin J, Chang J, Ha H, et al. Antigen glycosylation regulates efficacy of CAR T cells targeting CD19. Nat Commun 2022; 13:3367.

28. Morgan R, Gao G, Pawling J, Dennis JW, Demetriou M, Li B. N-acetylglucosaminyltransferase V (Mgat5)-mediated N-glycosylation negatively regulates Th1 cytokine production by T cells. J Immunol Baltim Md 1950 2004; 173:7200–8.

bioRxiv preprint doi: https://doi.org/10.1101/2023.01.23.525164; this version posted January 23, 2023. The copyright holder for this preprint (which was not certified by peer review) is the author/funder, who has granted bioRxiv a license to display the preprint in perpetuity. It is made available under aCC-BY-NC-ND 4.0 International license.

29. Smith LK, Boukhaled GM, Condotta SA, Mazouz S, Guthmiller JJ, Vijay R, Butler NS, Bruneau J, Shoukry NH, Krawczyk CM, et al. Interleukin-10 Directly Inhibits CD8+ T Cell Function by Enhancing N-Glycan Branching to Decrease Antigen Sensitivity. Immunity 2018; 48:299-312.e5.

30. Cedeno-Laurent F, Opperman M, Barthel SR, Hays D, Schatton T, Zhan Q, He X, Matta KL, Supko JG, Frank MH, et al. Metabolic inhibition of galectin-1-binding carbohydrates accentuates anti-tumor immunity. J Invest Dermatol 2012; 132:410–20.

31. Ye L, Park JJ, Dong MB, Yang Q, Chow RD, Peng L, Du Y, Guo J, Dai X, Wang G, et al. In vivo CRISPR screening in CD8 T cells with AAV– Sleeping Beauty hybrid vectors identifies membrane targets for improving immunotherapy for glioblastoma. Nat Biotechnol 2019; 37:1302–13.

32. Gurusamy D, Henning AN, Yamamoto TN, Yu Z, Zacharakis N, Krishna S, Kishton RJ, Vodnala SK, Eidizadeh A, Jia L, et al. Multi-phenotype CRISPR-Cas9 Screen Identifies p38 Kinase as a Target for Adoptive Immunotherapies. Cancer Cell 2020; 37:818-833.e9.

33. Hsiau T, Conant D, Rossi N, Maures T, Waite K, Yang J, Joshi S, Kelso R, Holden K, Enzmann BL, et al. Inference of CRISPR Edits from Sanger Trace Data. 2019.

34. Laroy W, Contreras R, Callewaert N. Glycome mapping on DNA sequencing equipment. Nat Protoc 2006; 1:397–405.

35. Yang M, Tang X, Zhang Z, Gu L, Wei H, Zhao S, Zhong K, Mu M, Huang C, Jiang C, et al. Tandem CAR-T cells targeting CD70 and B7-H3 exhibit potent preclinical activity against multiple solid tumors. Theranostics 2020; 10:7622–34.

36. Rizopoulos D. Generalized Linear Mixed Models using Adaptive Gaussian Quadrature [Internet]. 2022. Available from: https://CRAN.R-project.org/package=GLMMadaptive

37. R Core Team. A Language and environment for statistical computing [Internet]. Vienna, Austria: R Foundation for Statistical Computing; 2022. Available from: https://www.R-project.org/

38. Hartig F. DHARMa: Residual Diagnostics for Hierarchical (Multi-Level / Mixed) Regression Models. [Internet]. Available from: https://CRAN.R-project.org/package=DHARMa

39. Hothorn T, Bretz F, Westfall P. Simultaneous Inference in General Parametric Models.

40. Venables WN, Ripley BD. Modern Applied Statistics with S. Fourth Edition. Springer, New York: 2002.

41. Lüdecke D. ggefects: Tidy Data Frames of Marginal Effects from Regression Models. 2018.

42. Therneau T. A Package for Survival Analysis in R [Internet]. 2022. Available from: https://CRAN.R-project.org/package=survival

43. Therneau T, Grambsch P. Modeling Survival Data: Extending the Cox Model. Springer, New York: 2000.

44. Kassambra A, Kosinski M, Biecek P. Survminer: Drawing Survival Cuvres using “ggplot2” [Internet]. 2021. Available from: https://CRAN.R-project.org/package=survminer

45. Bates D, Maechler M, Bolker B, Walker S. Fitting Linear Mixed-Effects Models Using Lme4. 2015.

46. Nash JC, Varadhan R. Unifying Optimization Algorithms to Aid Software System Users: optimx for R. J Stat Softw 2011; 43:1–14.

bioRxiv preprint doi: https://doi.org/10.1101/2023.01.23.525164; this version posted January 23, 2023. The copyright holder for this preprint (which was not certified by peer review) is the author/funder, who has granted bioRxiv a license to display the preprint in perpetuity. It is made available under aCC-BY-NC-ND 4.0 International license.

730 47. Pustejovsky J. ClubSandwich: Cluster-Robust (Sandwich) Variance Estimators with Small-Sample
731 Corrections [Internet]. 2022. Available from: https://CRAN.R-project.org/package=clubSandwich

732

bioRxiv preprint doi: https://doi.org/10.1101/2023.01.23.525164; this version posted January 23, 2023. The copyright holder for this preprint (which was not certified by peer review) is the author/funder, who has granted bioRxiv a license to display the preprint in perpetuity. It is made available under aCC-BY-NC-ND 4.0 International license.

733 # Tables

734 **Table 1** | PCR primers to amplify the CRISPR target site. The forward primers were used for Sanger
735 Sequencing

Primer name	Primer Sequence (5' → 3')
MGAT5 Validation primer Fw	TCACAGCAGAATGGAAGT
MGAT5 Validation primer Rev	ACTGCTTATGAAGGCAGTGG

736

bioRxiv preprint doi: https://doi.org/10.1101/2023.01.23.525164; this version posted January 23, 2023. The copyright holder for this preprint (which was not certified by peer review) is the author/funder, who has granted bioRxiv a license to display the preprint in perpetuity. It is made available under aCC-BY-NC-ND 4.0 International license.

Figures

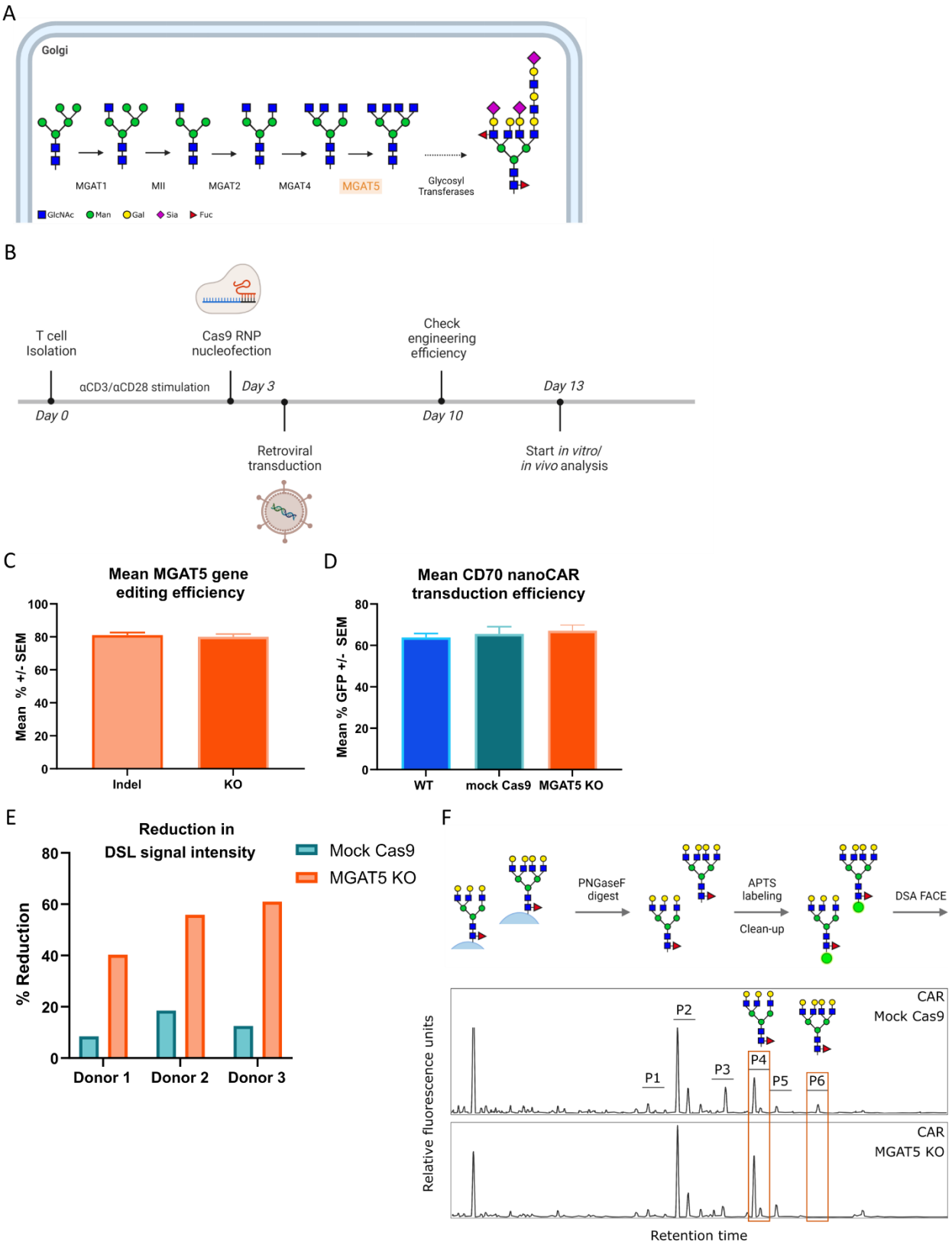

bioRxiv preprint doi: https://doi.org/10.1101/2023.01.23.525164; this version posted January 23, 2023. The copyright holder for this preprint (which was not certified by peer review) is the author/funder, who has granted bioRxiv a license to display the preprint in perpetuity. It is made available under aCC-BY-NC-ND 4.0 International license.

Figure 1 | MGAT5 glyco-gene editing and CD70 nanoCAR engineering. A. Pathway of N-glycan branching. N-glycan branching is achieved through a series of mannosidase (M) and mannosylglycoprotein-N-acetylglucosaminyltransferase (MGAT)-mediated reactions. The enzyme of interest to our project is marked in orange. This branching primarily occurs in the medial-Golgi compartment. In later compartments, branched glycans are acted upon by other enzymes including Gal-, GlcNAc-, sialyl- and fucosyltransferases to result in complex glycans. **B.** Experimental timeline. **C.** Mean editing efficiency as % insertions/deletions (indels) or proportion of indels that indicate a frameshift or are 21+ bp in length (assumes all edits are in a coding region) (KO) obtained for the Mgat5 locus. **D.** Mean transduction efficiency as % GFP expressing cells for the different engineering conditions. SEM: standard error of the mean. **E and F.** Profiling of alterations in cell surface glycosylation upon MGAT5 KO in CD70 nanoCAR T cells. **E.** Lectin staining. 2 x 10^5 wild type, mock engineered (green) or MGAT5 KO (orange) CAR T cells were collected, stained with fixable viability dye eFl780 and biotinylated lectin followed by secondary staining with PE-coupled neutravidin. Analysis was done by flow cytometry and graphs show the reduction in lectin binding signal intensities as compared to wild type CAR T cells after gating on viable cells. Results are shown for engineered T cells from three independent blood donors. **F.** DSA-FACE profiling. Schematic representation of the sample preparation and DSA-FACE profiles of the cell-surface glycome of mock engineered and MGAT5 KO CAR T cells. Sialidase digest was performed on the samples prior to the analysis. The major pairs of peaks in the profile are annotated P1-P6.

bioRxiv preprint doi: https://doi.org/10.1101/2023.01.23.525164; this version posted January 23, 2023. The copyright holder for this preprint (which was not certified by peer review) is the author/funder, who has granted bioRxiv a license to display the preprint in perpetuity. It is made available under aCC-BY-NC-ND 4.0 International license.

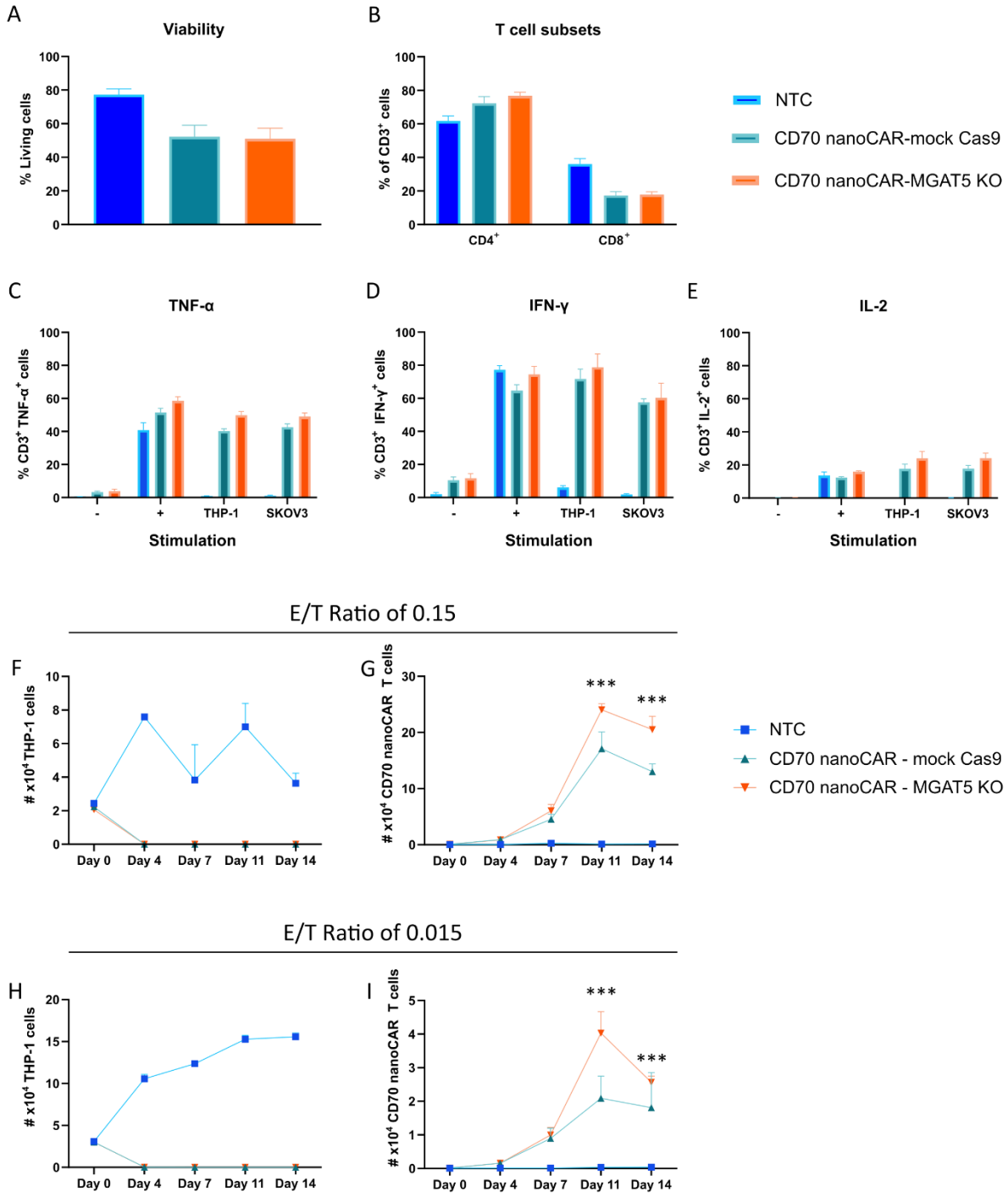

Figure 2 | The impact of glyco-engineering in MGAT5 on in vitro CD70 nanoCAR efficacy. A. and B. Effect of MGAT5 KO on CD70 nanoCAR viability and subset distribution at day 13 of in vitro culturing. MGAT5 KO CD70 nanoCAR T cells were generated as described above. At day 13, the immunophenotype of the cells was evaluated prior to the initiation of the functional assays. Mean data is shown from experiments performed with three independent donors. Error bars represent the standard error of the mean (SEM). **C-E.** The impact of glyco-engineering of MGAT5 on in vitro CD70 nanoCAR cytokine production. Cytokine production of glyco-engineered CD70 nanoCAR T cells was evaluated by intracellular staining after co-incubation with THP-1 and SKOV3 target cell lines for 16 hours. Unstimulated cells were included as

bioRxiv preprint doi: https://doi.org/10.1101/2023.01.23.525164; this version posted January 23, 2023. The copyright holder for this preprint (which was not certified by peer review) is the author/funder, who has granted bioRxiv a license to display the preprint in perpetuity. It is made available under aCC-BY-NC-ND 4.0 International license.

negative control (-) while Immunocult stimulation was included as positive control (+). Technical duplicates were analyzed. Mean percentages of TNF-α, IFN-γ and IL-2 positive $CD3^+$ are shown. Mean data is shown from experiments performed with three independent donors. Error bars represent the standard error of the mean (SEM). **F-I.** The impact of glyco-engineering in MGAT5 on in vitro CD70 nanoCAR cytotoxic potential. Glyco-engineered CD70 nanoCAR T cells cultured in the presence of IL-7 and IL-15 were incubated at different effector to target THP-1 cell ratios in duplicate and cell numbers were analyzed over a time period of 14 days. A second challenge with THP-1 cells was added at day 7. Error bars represent the standard error of the mean cell number from data obtained with 3 different T cell donors. **F and G.** Results for E/T ratio of 0.15 corresponding to the co-culture of 20 000 THP-1 cells with 3 000 glyco-engineered CD70 nanoCAR T cells**. H and I.** Results for E/T ratio of 0.015 corresponding to the co-culture of 20 000 THP-1 cells with 300 CD70 nanoCAR T cells. The data from the right panels was modeled using a mixed negative binomial model with a random intercept for each cluster (a cluster being defined as the set of measurements sharing the same donor, E/T Ratio and type of CAR T cells). *** $p<0.001$.

bioRxiv preprint doi: https://doi.org/10.1101/2023.01.23.525164; this version posted January 23, 2023. The copyright holder for this preprint (which was not certified by peer review) is the author/funder, who has granted bioRxiv a license to display the preprint in perpetuity. It is made available under aCC-BY-NC-ND 4.0 International license.

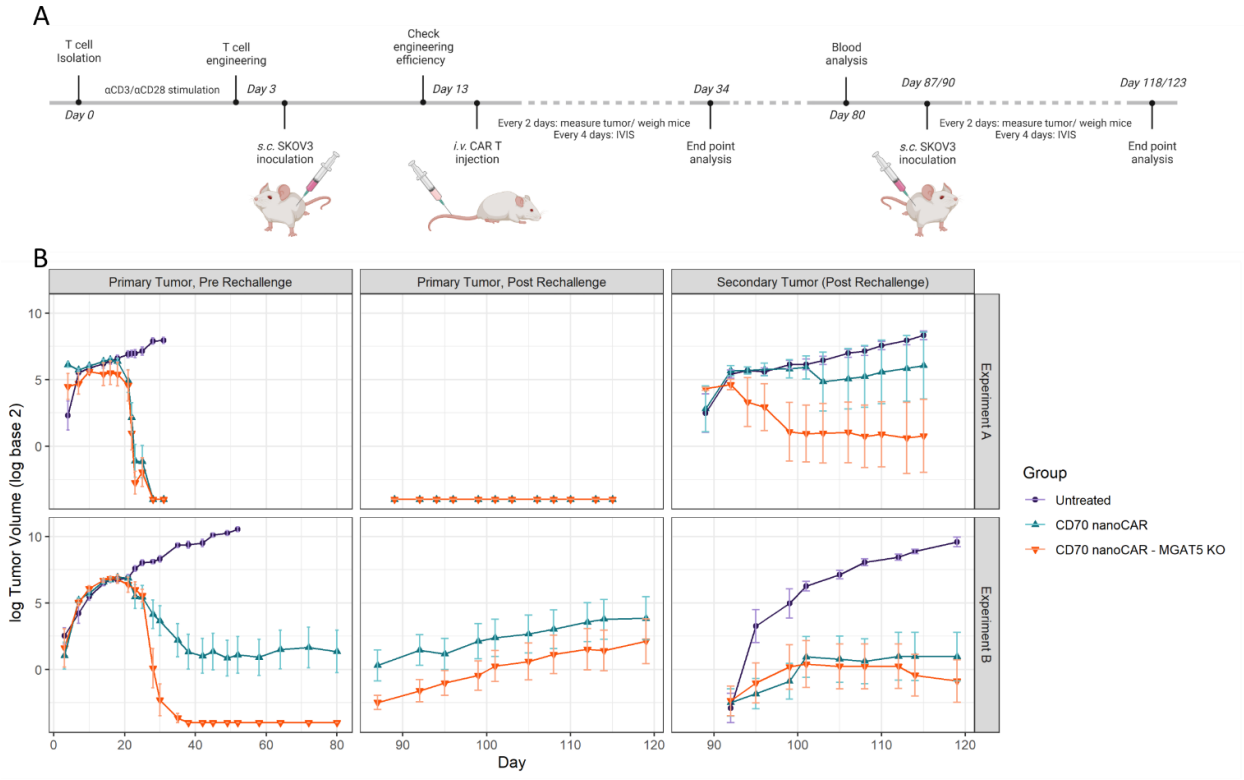

C

Treatment group	Outcome	Cases	Total	%
Untreated	No Control	28	28	100.0
	Partial control, relapse	0		0.0
	Control, relapse	0		0.0
	Control, no relapse	0		0.0
CD70 nanoCAR	No Control	5	30	16.7
	Partial control, relapse	3		10.0
	Control, relapse	7		23.3
	Control, no relapse	15		50.0
CD70 nanoCAR – MGAT5 KO	No Control	0	21	0.0
	Partial control, relapse	0		0.0
	Control, relapse	6		26.6
	Control, no relapse	15		71.4

D

Treatment group	Outcome	Cases	Total	%
Untreated	No Control	18	18	100.0
	Partial control	0		0.0
	Control	0		0.0
CD70 nanoCAR	No Control	8	17	47.0
	Partial control	1		5.9
	Control	8		47.0
CD70 nanoCAR – MGAT5 KO	No Control	2	14	14.0
	Partial control	3		21.0
	Control	9		64.0

Figure 3 | The impact of glyco-engineering on in vivo CD70 nanoCAR functionality. A. Schematic representation of the experimental timeline for the study of the in vivo efficacy of MGAT5 KO CD70 nanoCAR T cells. Timepoints that differ between Experiment A and Experiment B are indicated with a '/'. **B.** Tumor burden measured by caliper. Tumor volume is calculated as (tumor length x tumor width^2)/2. Group means are indicated with error bars representing the standard error of the mean (SEM). **C.** Overview of the response to primary tumor challenge in the different treatment groups for both experiments combined. **D.** Overview of the response to secondary tumor challenge in the different treatment groups for both experiments combined.

bioRxiv preprint doi: https://doi.org/10.1101/2023.01.23.525164; this version posted January 23, 2023. The copyright holder for this preprint (which was not certified by peer review) is the author/funder, who has granted bioRxiv a license to display the preprint in perpetuity. It is made available under aCC-BY-NC-ND 4.0 International license.

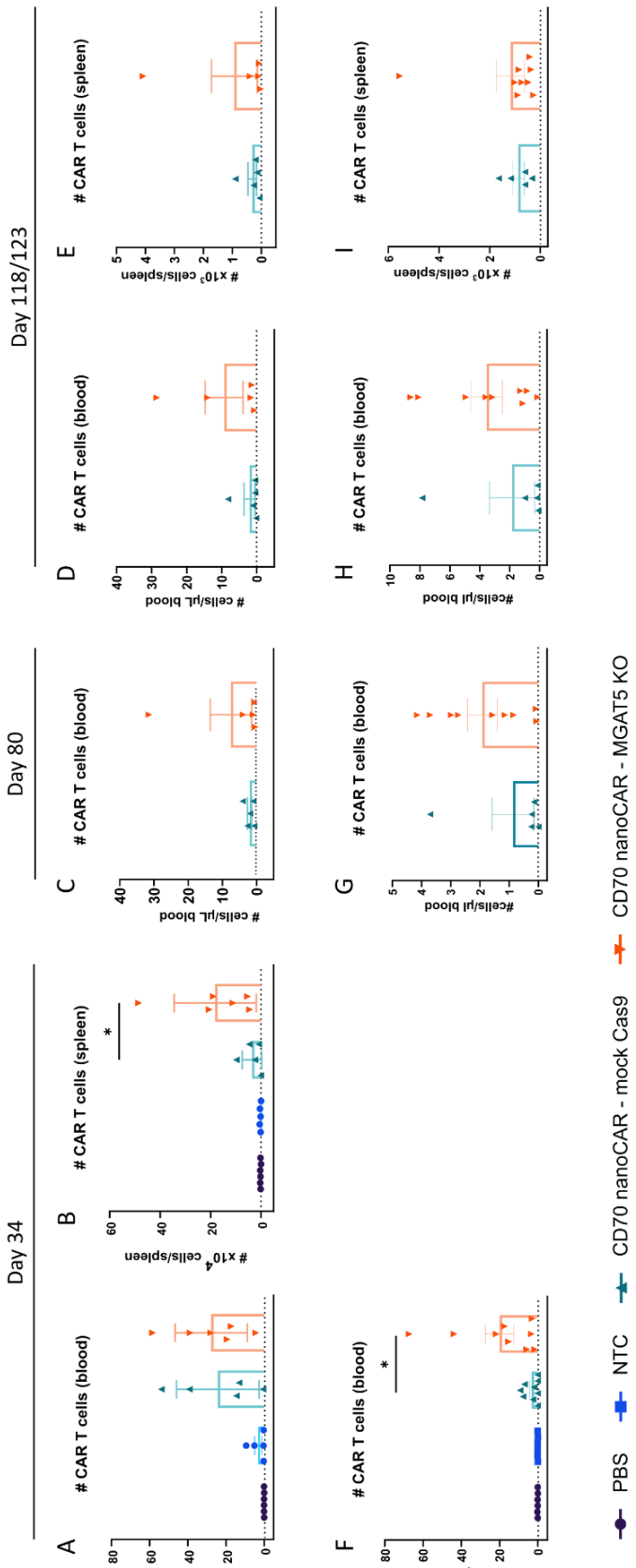

Figure 4| Flow cytometry-based analysis of CART cells in blood and spleen. Immunophenotype of mock Cas9 or MGAT5 KO CD70 nanoCAR T cells in peripheral blood and spleen at day 34, day 80 and day 118 (Experiment A)/day 123 (Experiment B). Data is represented as proportion of $CD3^+GFP^+$ cells. Each data point represents a single animal. Error bars represent the standard error of the mean (SEM). P-values were calculated by a one-way ANOVA:*, $P < 0.05$ **A, C, D, F, G, H.** The number of CART T cells present in the blood is indicated as cells/µL blood. **B, E, I.** The number of CAR T cells in the spleen is indicated as $CD4^+$ or $CD8^+$ T cells.

bioRxiv preprint doi: https://doi.org/10.1101/2023.01.23.525164; this version posted January 23, 2023. The copyright holder for this preprint (which was not certified by peer review) is the author/funder, who has granted bioRxiv a license to display the preprint in perpetuity. It is made available under aCC-BY-NC-ND 4.0 International license.

Supplementary information

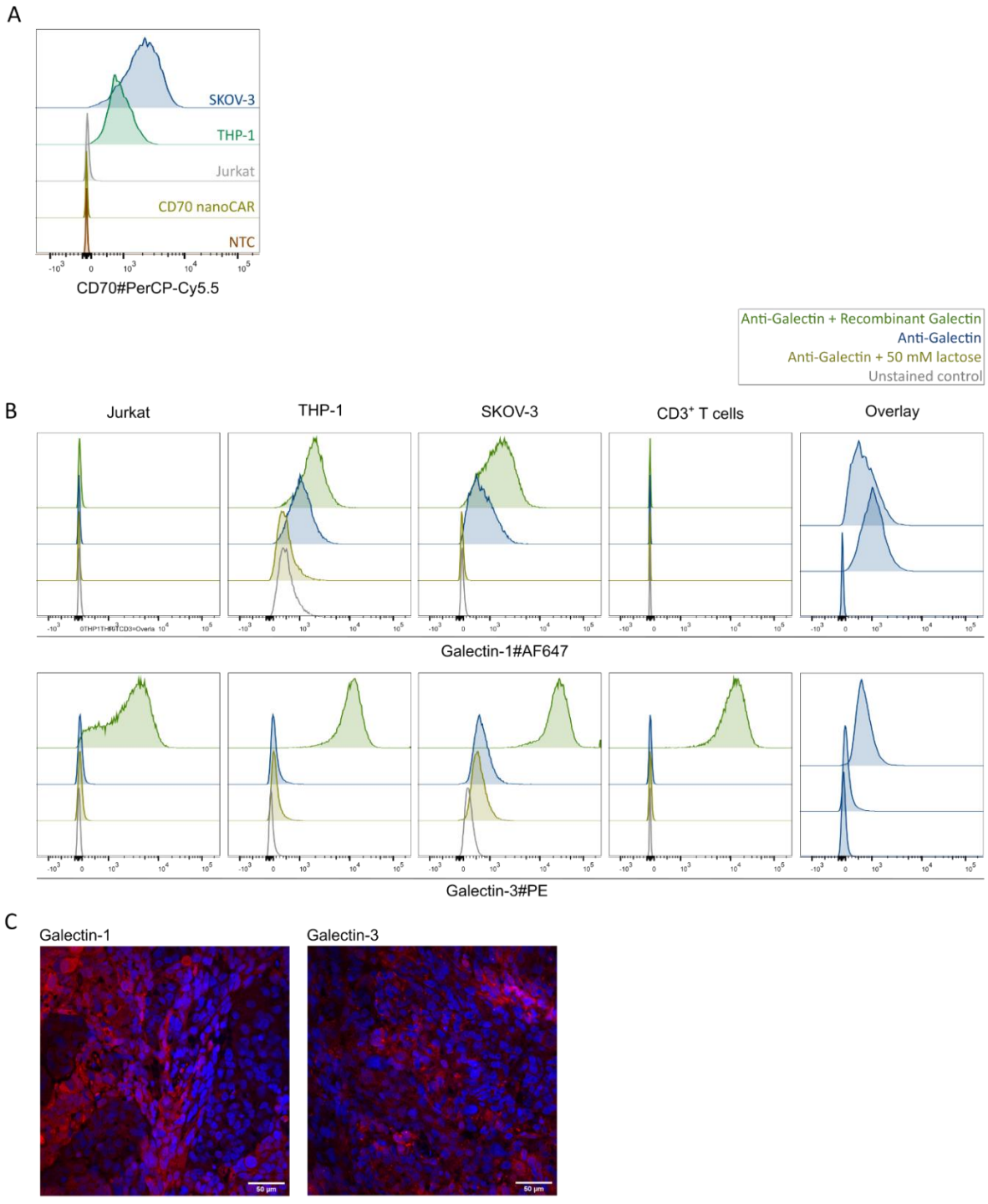

Supplementary Figure 1 | Characterization of the THP-1 and SKOV-3 cell lines used as target cells. **A.** CD70 antigen expression on the THP-1 and SKOV-3 target cell lines was evaluated by flow cytometry. Jurkat cells were included as negative control. Non-transduced control (NTC) and CD70 nanoCAR expressing human T cells were included to check for auto-antigen expression. **B.** Evaluation of the secretion of Galectins by the tumor cell lines under study. Secretion and cell surface binding of Galectin-1 and Galectin-3 by different cell types was assessed by flow cytometry. Jurkat cells were included as negative controls. As a control,

bioRxiv preprint doi: https://doi.org/10.1101/2023.01.23.525164; this version posted January 23, 2023. The copyright holder for this preprint (which was not certified by peer review) is the author/funder, who has granted bioRxiv a license to display the preprint in perpetuity. It is made available under aCC-BY-NC-ND 4.0 International license.

799 lactose was used as competitive inhibitor to reduce cell surface galectin binding. Additionally, cells were
800 incubated with recombinant galectins as positive control. The secretion and cell surface binding of
801 Galectin-1 and Galectin-3 on THP-1 and SKOV-3 cells are summarized in the overlaid histograms. Results
802 representative for two independent experiments are shown. C. Representative images of an FFPE tumor
803 sample expressing Galectin-1 (left) and Galectin-3 (right) at a 25x magnification (red) with DAPI nuclear
804 counterstain (blue).

bioRxiv preprint doi: https://doi.org/10.1101/2023.01.23.525164; this version posted January 23, 2023. The copyright holder for this preprint (which was not certified by peer review) is the author/funder, who has granted bioRxiv a license to display the preprint in perpetuity. It is made available under aCC-BY-NC-ND 4.0 International license.

A

Target	sgRNA Sequence (5′ → 3′)
Mock (scrambled sgRNA not targeting any gene)	GCACUACCAGAGCUAACUCA
MGAT5	GUGACUUUUGGCUUCAUUUG

B

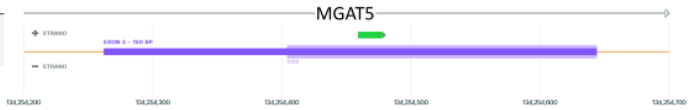

C

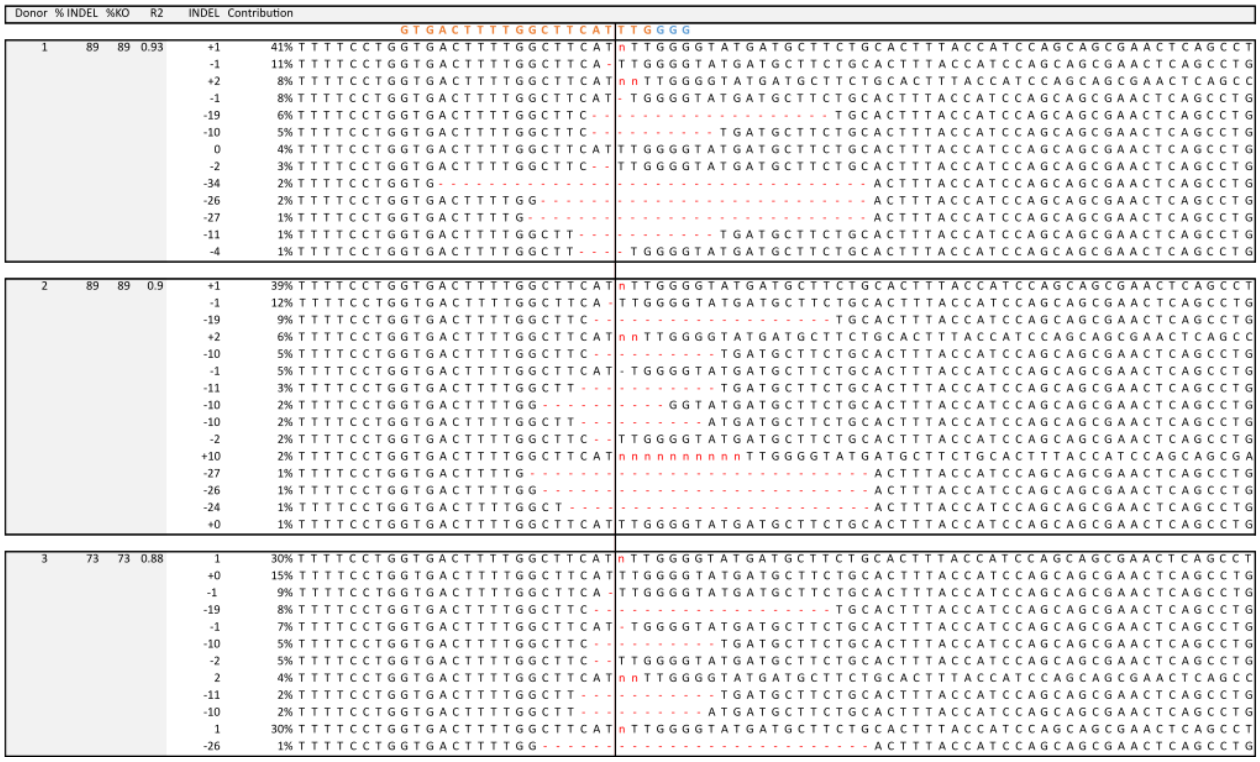

Supplementary Figure 2 | A. Overview of the gRNA used in this study to generate a knockout in MGAT5. **B.** Genome localization of the gRNA target site (green). **C.** Mutation patterns detected by Sanger sequencing and ICE analysis. sgRNA target sequence (orange) and PAM (blue) sequences are indicated above the corresponding traces. Red dashes denote deleted bases and red n indicate inserted nucleotides. The vertical black line corresponds to the predicted Cas9 cut site. The contribution shows the inferred fractions of each mutant sequence present in the edited population. Cutting and error-prone repair usually results in mixed sequencing bases after the cut. %INDEL: % insertions/deletions, %KO: proportion of indels that indicate a frameshift or are 21+ bp in length (assumes all edits are in a coding region), R2: model fit (how well the proposed indel distribution fits the Sanger sequence data of the edited sample). Representative results of three different donors are shown.

bioRxiv preprint doi: https://doi.org/10.1101/2023.01.23.525164; this version posted January 23, 2023. The copyright holder for this preprint (which was not certified by peer review) is the author/funder, who has granted bioRxiv a license to display the preprint in perpetuity. It is made available under aCC-BY-NC-ND 4.0 International license.

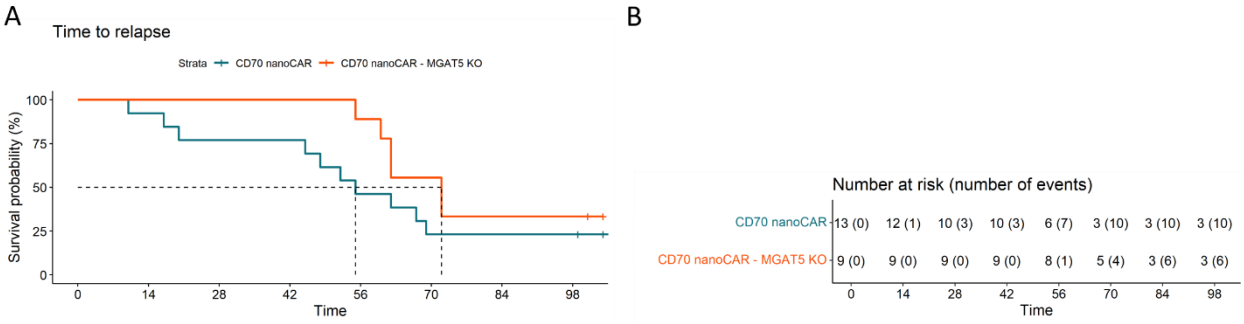

Supplementary Figure 3 | Time (in days) to relapse of the primary tumor (Experiment B). Time zero was set as the time that the primary tumor was controlled or partially controlled. An event is the time the tumor starts growing again. We take the last day before the tumor has increased in size again or became detectable again as the onset of relapse. **A.** Kaplan-Meier curve. This plot shows the probability of relapse-free survival in the two groups. The dotted lines indicate median survival times. **B.** Risk and event table corresponding to the Kaplan-Meier plot. The table shows the number of mice at risk and, between brackets, the cumulative number of relapses in each group and at each time.

bioRxiv preprint doi: https://doi.org/10.1101/2023.01.23.525164; this version posted January 23, 2023. The copyright holder for this preprint (which was not certified by peer review) is the author/funder, who has granted bioRxiv a license to display the preprint in perpetuity. It is made available under aCC-BY-NC-ND 4.0 International license.

A

Parameter	Estimate	S.E.	Statistic	Adj. p-value
Intercept	5.660	0.297	19.029	<0.001
Time 7	0.077	0.035	2.221	0.147
Time 19	0.038	0.075	0.510	0.995
Time 26	0.013	0.073	0.185	1
Group CD70 nanoCAR	0.013	0.264	0.390	0.999
Group CD70 nanoCAR – MGAT5 KO	-0.780	0.619	-1.261	0.711
Time 19 : Group CD70 nanoCAR	-1595	0.149	-10.704	<0.001
Time 19 : Group CD70 nanoCAR – MGAT5 KO	-1.601	0.128	-12.526	<0.001
Time 26 : Group CD70 nanoCAR	1.386	0.423	3.274	0.007
Time 26 : Group CD70 nanoCAR – MGAT5 KO	1.614	0.321	5.029	<0.001
Random intercept S.D. (ID = mouse)	1.127			
Residual S.D.	1.906			

B

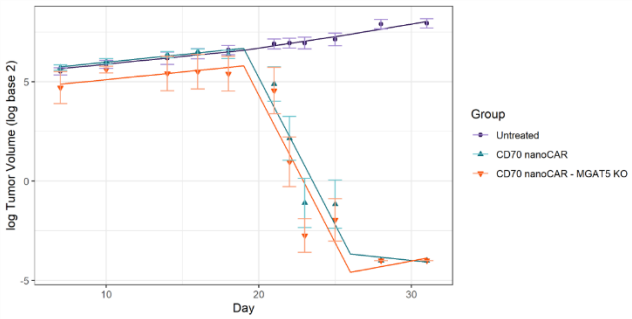

C

Contrast	Daily change (%)	Estimate	95% CI (lower)	95% CI (upper)	Adj. p-value
Baseline ratio of tumor sizes, CD70 nanoCAR and CD70 nanoCAR – MGAT5 KO average over Untreated	NA	0.79	0.41	1.53	0.846
Growth rate day 7-19, all treatment groups	6.0	1.06	0.99	1.12	0.124
Growth rate day 19-26, Untreated	8.0	1.08	1.00	1.17	0.032
Growth rate day 19-26, CD70 nanoCAR	-64.0	0.36	0.28	0.47	<0.001
Growth rate day 19-26, CD70 nanoCAR-MGAT5 KO	-64.0	0.36	0.28	0.46	<0.001
Ratio of growth rate day 19-26 CD70 nanoCAR/MGAT5 KO over Untreated	NA	0.33	0.28	0.39	<0.001
Ratio of growth rate day 19-26 CD70 nanoCAR over CD70 nanoCAR- MGAT5 KO	NA	1.00	0.70	1.41	1

Supplementary Figure 4 | Longitudinal analysis of the primary tumor (Experiment A). Using the longitudinal data of the primary tumors in Experiment A, a piecewise linear mixed model with the first timepoint at day 7 and knots at day 19 and 26 and with interactions between the group and the first and second time-segment was fitted, which allows to model the mean traces of each treatment group. **A.** Summary of the model output, listing all parameter estimates for the model logTumorVol ~ Time7 + (Time19 + Time26))*Group + (1 | ID). The table gives parameters and standard errors on the ^{2}log scale together with test statistics and multiple testing adjusted p-values (null hypothesis: parameter equal to zero). **B.** Plot of the caliper measurements and model fit. The dots are mean ^{2}log tumor volumes with S.E.M. for each group at each day they were measured. The lines are the model-based predictions for the mean ^{2}log tumor volume for each group. **C.** Inference for different research questions. In this table, the estimates and confidence intervals are transformed back to the original scale so we can interpret them in a straightforward way. E.g. a growth rate of 1.06 means a multiplicative change in tumor volume of 1.06 each day, or a 6% increase each day, compared to the previous day. In this context, the adjusted p-values also relate to a transformed null hypothesis (i.e. estimate equals one). S.E.: Standard Error. CI: Confidence Interval.

bioRxiv preprint doi: https://doi.org/10.1101/2023.01.23.525164; this version posted January 23, 2023. The copyright holder for this preprint (which was not certified by peer review) is the author/funder, who has granted bioRxiv a license to display the preprint in perpetuity. It is made available under aCC-BY-NC-ND 4.0 International license.

A

Parameter	Estimate	S.E.	Statistic	Adj. p-value
Intercept	4.129	0.578	7.145	<0.001
Time 89	0.167	0.019	8.885	<0.001
Group CD70 nanoCAR	0.611	0.797	0.767	0.923
Group CD70 nanoCAR – MGAT5 KO	-0.248	0.998	-0.248	1
Time 89 : Group CD70 nanoCAR	-0.120	0.120	-0.998	0.809
Time 89 : Group CD70 nanoCAR – MGAT5 KO	-0.321	0.102	-3.137	0.009
Random intercept S.D. (ID = mouse)	1.571			
Random slope time89 S.D. (ID = mouse)	0.198			
Correlation random intercept and slope	-0.292			
Residual S.D.	1.361			

B

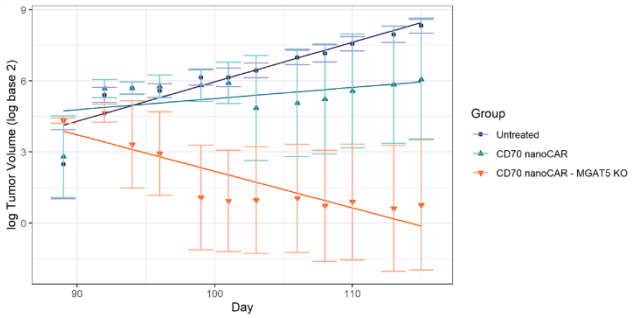

C

Contrast	Daily change (%)	Estimate	95% CI (lower)	95% CI (upper)	Adj. p-value
Growth rate Untreated	12.0	1.12	1.09	1.16	<0.001
Growth rate CD70 nanoCAR	3.0	1.03	0.85	1.26	0.973
Growth rate CD70 nanoCAR – MGAT5 KO	-10.0	0.90	0.76	1.07	0.355
Ratio of growth rate CD70 nanoCAR over CD70 nanoCAR – MGAT5 KO	NA	0.87	0.67	1.13	0.505

Supplementary Figure 5 | Longitudinal analysis of the secondary tumor (Experiment A). A linear mixed model with interactions between the group and time was fitted to the longitudinal data of the secondary tumor in Experiment A, which start at day 89. **A.** Summary of the model output, listing all parameter estimates for the model logTumorVol ~ Time89*Group + (Time89 | ID). The table gives parameters and standard errors on the ^{2}log scale together with test statistics and multiple testing adjusted p-values (null hypothesis: parameter equal to zero). **B.** Plot of the caliper measurements and model fit. The dots are mean ^{2}log tumor volumes with S.E.M. for each group at each day they were measured. The lines are the model-based predictions for the mean ^{2}log tumor volume for each group. **C.** Inference for different research questions. In this table, the estimates and confidence intervals are transformed back to the original scale so we can interpret them in a straightforward way. S.E.: Standard Error. CI: Confidence Interval.

bioRxiv preprint doi: https://doi.org/10.1101/2023.01.23.525164; this version posted January 23, 2023. The copyright holder for this preprint (which was not certified by peer review) is the author/funder, who has granted bioRxiv a license to display the preprint in perpetuity. It is made available under aCC-BY-NC-ND 4.0 International license.

A

Parameter	Estimate	S.E.	Statistic	Adj. p-value
Intercept	4.973	0.360	13.823	<0.001
Time 7	0.151	0.025	5.974	<0.001
Time 21	-0.0019	0.036	-0.525	0.996
Time 33	-0.055	0.023	-2.410	0.098
Group CD70 nanoCAR	0.262	0.321	0.816	0.952
Group CD70 nanoCAR – MGAT5 KO	0.398	0.338	1.179	0.781
Time 21 : Group CD70 nanoCAR	-0.623	0.097	-6.404	<0.001
Time 21 : Group CD70 nanoCAR – MGAT5 KO	-1.095	0.037	-29.292	<0.001
Time 33 : Group CD70 nanoCAR	0.578	0.098	5.914	<0.001
Time 33: Group CD70 nanoCAR – MGAT5 KO	1.019	0.044	22.979	<0.001
Random intercept S.D. (ID = mouse)	1.074			
Random slope Time7 S.D. (ID = mouse)	0.087			
Correlation random intercept and slope	-0.348			
Residual S.D.	1.67			

B

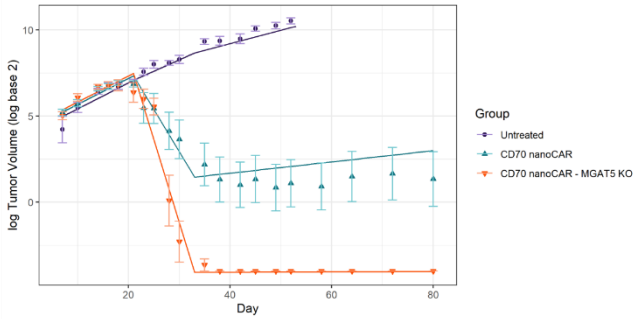

C

Contrast	Daily change (%)	Estimate	95% CI (lower)	95% CI (upper)	Adj. p-value
Baseline ratio of tumor sizes, CD70 nanoCAR and CD70 nanoCAR – MGAT5 KO average over Untreated	NA	1.26	0.71	2.22	0.897
Growth rate day 7-21, all treatment groups	11.0	1.11	1.06	1.17	<0.001
Growth rate day 22-33, Untreated	10.0	1.10	1.06	1.13	<0.001
Growth rate day 33-84, Untreated	6.0	1.06	1.03	1.08	<0.001
Growth rate day 22-33, CD70 nanoCAR	-29.0	0.71	0.59	0.86	<0.001
Growth rate day 33-84, CD70 nanoCAR	2.0	1.02	0.97	1.08	0.995
Growth rate day 22-33, CD70 nanoCAR – MGAT5 KO	-49.0	0.51	0.48	0.55	<0.001
Growth rate day 33-84, CD70 nanoCAR – MGAT5 KO	0.0	1.00	0.96	1.04	1
Ratio of average growth rate day 22-32 CD70 nanoCAR/ MGAT5 KO over Untreated	NA	0.55	0.50	0.61	<0.001
Ratio of growth rate day 22-32 CD70 nanoCAR over CD70 nanoCAR – MGAT5 KO	NA	0.72	0.59	0.88	<0.001
Ratio of average growth rate day 33-84 CD70 nanoCAR/ MGAT5 KO over Untreated	NA	0.96	0.92	1.0	<0.001
Ratio of growth rate day 33-84 CD70 nanoCAR over CD70 nanoCAR – MGAT5 KO	NA	0.98	0.91	1.05	0.981
Tumor volume day 60, CD70 nanoCAR	NA	5.07	0.32	80.07	<0.001

Supplementary Figure 6 | Longitudinal analysis of the primary tumor (Experiment *B*). A piecewise linear mixed model with interactions between the group and the second- and third-time segment was fitted to the longitudinal data of the primary tumor in Experiment B. The data start at day 7 and knots are added at day 21 and 33. **A.** Summary of the model output, listing all parameter estimates for the model logTumorVol ~ Time7+(Time21+Time33)*Group + (Time7 | ID). The table gives parameters and standard errors on the ^{2}log scale together with test statistics and multiple testing adjusted p-values (null hypothesis: parameter equal to zero). **B.** Plot of the caliper measurements and model fit. The dots are mean ^{2}log tumor volumes with S.E.M. for each group at each day they were measured. The lines are the model-based predictions for the mean ^{2}log tumor volume for each group. **C.** Inference for different research questions. In this table, the estimates and confidence intervals are transformed back to the original scale so we can interpret them in a straightforward way. S.E.: Standard Error. CI: Confidence Interval.

bioRxiv preprint doi: https://doi.org/10.1101/2023.01.23.525164; this version posted January 23, 2023. The copyright holder for this preprint (which was not certified by peer review) is the author/funder, who has granted bioRxiv a license to display the preprint in perpetuity. It is made available under aCC-BY-NC-ND 4.0 International license.

A

Parameter	Estimate	S.E.	Statistic	Adj. p-value
Intercept	0.897	0.700	1.282	0.428
Time	0.158	0.022	7.077	<0.001
Group CD70 nanoCAR – MGAT5 KO	-2.126	0.881	-2.415	0.041
Random intercept S.D. (ID = mouse)	2.047			
Random slope time S.D. (ID = mouse)	0.083			
Correlation random intercept and slope	-0.434			
Residual S.D.	1.251			

B

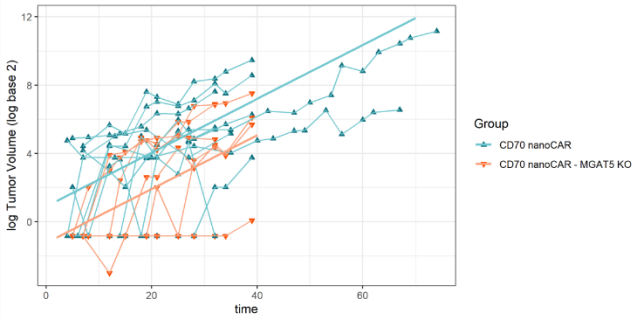

C

Contrast	Daily change (%)	Estimate	95% CI (lower)	95% CI (upper)	Adj. p-value
Average ratio in tumor volume, CD70 nanoCAR over CD70nanoCAR – MGAT5 KO	NA	4.37	1.12	17.08	0.031
Growth rate CD70 nanoCAR and CD70 nanoCAR – MGAT5 KO	12	1.12	1.08	1.15	<0.001

Supplementary Figure 7 | Longitudinal analysis of the relapse of the primary tumor (Experiment B). A linear mixed model was fitted to the longitudinal data of the relapsing mice in Experiment B. Only mice in the treated groups had cleared the tumors fully or partially, so the analysis is naturally restricted to the two CAR groups. To enable this analysis, we also had to change the timescale for each individual mouse such that the first day of the relapse became day 0. Had we not done this, the analysis would be moot since, on average, the CD70 nanoCAR group had relapses earlier than the CD70 nanoCAR – MGAT5 KO group. This would almost automatically result in larger tumors in the CD70 nanoCAR group compared to the CD70 nanoCAR – MGAT5 KO group. **A.** Summary of the model output, listing all parameter estimates for the model logTumorVol ~ Time+Group + (Time | ID). The table gives parameters and standard errors on the ^{2}log scale together with test statistics and multiple testing adjusted p-values (null hypothesis: parameter equal to zero). **B.** Plot of the caliper measurements and model fit. The dots are individual ^{2}log tumor volumes. Dots connected by a line are measurements from the same mouse (note that due to the time translation, mean values per day are not informative, since not all measurements were made on the same day on the new timescale). The two straight lines are the model-based predictions for the mean ^{2}log tumor volume for each group. **C.** Inference for different research questions. In this table, the estimates and confidence intervals are transformed back to the original scale so we can interpret them in a straightforward way. Note that the interaction between Time and Group was not significant here so the growth rate is the same in each group but the tumors are smaller on average in the MGAT KO group. S.E.: Standard Error. CI: Confidence Interval.

bioRxiv preprint doi: https://doi.org/10.1101/2023.01.23.525164; this version posted January 23, 2023. The copyright holder for this preprint (which was not certified by peer review) is the author/funder, who has granted bioRxiv a license to display the preprint in perpetuity. It is made available under aCC-BY-NC-ND 4.0 International license.

A

Parameter	Estimate	S.E.	Statistic	Adj. p-value
Intercept	-0.759	0.982	-0.773	0.936
Time 92	00824	0.105	7.823	<0.001
Time 101	-0.694	0.110	-6.314	<0.001
Group CD70 nanoCAR	-1.503	0.862	-1.743	0.345
Group CD70 nanoCAR – MGAT5 KO	0.027	0.892	0.030	1
Time 101 : Group CD70 nanoCAR	-0.047	0.101	-0.461	0.994
Time 101 : Group CD70 nanoCAR – MGAT5 KO	-0.282	0.192	-1.471	0.522
Random intercept S.D. (ID = mouse)	2.851			
Random slope time92 S.D. (ID = mouse)	0.21			
Correlation random intercept and slope	-0.817			
Residual S.D.	2.230			

B

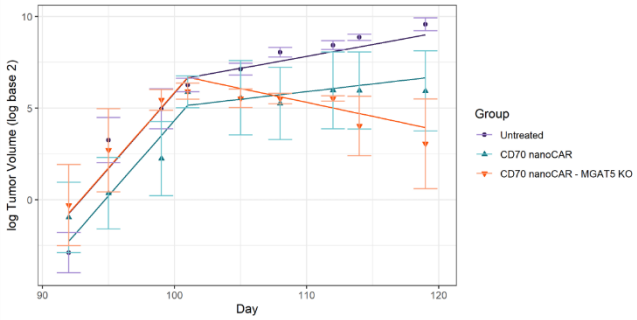

C

Contrast	Daily change (%)	Estimate	95% CI (lower)	95% CI (upper)	Adj. p-value
Growth rate day 92-101, all treatment groups	77.0	1.77	1.47	2.13	<0.001
Growth rate day 101-121, Untreated	9.0	1.09	1.01	1.19	0.018
Growth rate day 101-121, CD70 nanoCAR	6.0	1.06	0.90	1.25	0.845
Growth rate day 101-121, CD70 nanoCAR – MGAT5 KO	-10.0	0.90	0.66	1.23	0.855
Ratio of growth rate day 101-121, CD70 nanoCAR over CD70 nanoCAR – MGAT5 KO	NA	0.85	0.59	1.22	0.683

Supplementary Figure 8 |Longitudinal analysis of the secondary tumor (Experiment B). A piecewise linear mixed model with interactions between the group and the second time segment was fitted to the longitudinal data of the secondary tumor in Experiment B. The data start at day 92 and a knot is added at day 101. **A.** Summary of the model output, listing all parameter estimates for the model logTumorVol ~ Time92+Time101*Group + (Time92 | ID). The table gives parameters and standard errors on the ^{2}log scale together with test statistics and multiple testing adjusted p-values (null hypothesis: parameter equal to zero). **B.** Plot of the caliper measurements and model fit. The dots are mean ^{2}log tumor volumes with S.E.M. for each group at each day they were measured. The lines are the model-based predictions for the mean ^{2}log tumor volume for each group. **C.** Inference for different research questions. In this table, the estimates and confidence intervals are transformed back to the original scale so we can interpret them in a straightforward way. S.E.: Standard Error. CI: Confidence Interval.